J. Hydrol. Hydromech., 72, 2024, 1, 95–112
https://doi.org/10.2478/johh-2023-0042
© 2024 Stanislav Kotaška et al., published by Sciendo. This work is licensed under the Creative Commons Attribution-NonCommercial-NoDerivatives 4.0 International Licence.

sciendo Journal of Hydrology and Hydromechanics Institute of Hydrology SAS

# Spectral analysis of oscillatory wind wave parameters in fetch-limited deep-water conditions at a small reservoir and their prediction: Case Study of the Hulín Reservoir in the Czech Republic

Stanislav Kotaška[1*], David Duchan[1], Petr Pelikán[2], Miroslav Špano[1]

[1] Faculty of Civil Engineering, Institute of Water Structures, Brno University of Technology, Veveří 331/95, Brno, 602 00, Czech Republic.
[2] Department of Landscape Management, Faculty of Forestry and Wood Technology, Mendel University, Zemědělská 3, Brno, 613 00, Czech Republic.
[*] Corresponding author. E-mail: kotaska.s@fce.vutbr.cz

**Abstract**: The dams and banks of small water reservoirs face significant erosion from wind-generated oscillatory waves. Proper design of structure height is crucial to protect such banks against erosion, considering the maximum characteristics of wind waves. Long-term measurements at the Hulín reservoir revealed that the wave spectrum aligns best with the Bretschneider type. This spectrum serves as a basis for simulating oscillatory waves and their impact on shore protection structure design. Empirical models were evaluated using wind and wave data from Hulín reservoir in the Czech Republic. The measured wind speeds attained a maximum of 8 m/s, and wave heights reached up to 15 cm. The Bretschneider (SMB) empirical formula provided the most accurate estimation of wave height ($H_{m0}$), with an average underestimate of RMSE = 0.038 m. On the other hand, Wilson revisited (WIL rev.) performed less effectively, with an average RMSE = 0.304 m. For wave period ($T$) estimation, Bretschneider (SMB) yielded the best results, with an average RMSE = 0.062 s. Conversely, Wilson revisited (WIL rev.) showed poorer performance, with an average underestimate of RMSE = 2.196 s. The discrepancy between the empirical formulas and measured values, particularly in underestimating $H_{m0}$, can be attributed to inaccurate determination of fetch length and wind speed.

**Keywords:** Oscillatory waves; Spectral analysis; Spectral density; Small closed reservoir; Wave prediction.

## 1 INTRODUCTION

Most of the models used to calculate wave heights and periods are derived from long-term measurements of sea waves. These models are then also applied to small closed inland reservoirs, leading to the characteristic height and period then being overstated relative to the real incidence of wave height and period. The assumption is that small, closed reservoirs contain a spectrum that can be characterized by the JONSWAP model. However, evaluation of the existing models is necessary, because many of them have been calibrated on very large lakes or on the open sea.

In the Czech Republic (CR), the ČSN 75 0255 standard "Calculation of wave effects on reservoirs", which was issued in 1988 (CSN 75 0255, 1988), deals with the calculation of the effect of wind oscillatory waves on water structures and natural reservoir banks. The standard is based on information and the state of knowledge that existed 40 years ago. Since then, both the ability to measure and process data and the options for simulating the effects of waves on structures have expanded due to increased computing power and the proliferation of simulation software. Recommendations for draft measures to protect the structures and banks of reservoirs are also being extended as new materials and products are progressively developed, leading to the need to supplement current information on the effects of wave loads.

The standard ČSN 75 0255 (CSN 75 0255, 1988) relies on the assumption that simple sine waves form on reservoirs according to the linear theory of wave propagation, which is considered valid. In reality, however, a field of random waves is generated on reservoirs due to the action of the wind, spread across the water's surface. When certain conditions are met, it can be assumed that the relationships between wave parameters can still be sufficiently plausibly described by linear wave propagation theory. In the last decade in the Czech Republic, numerous types of research have been performed on closed reservoirs, and draft protective measures have been applied to banks (Kotaška, 2019; Pelikán and Marková, 2013; Pelikán and Šlezingr, 2015; Pelikán and Koutný, 2016; Pelikán et al., 2020; Říha and Špano, 2012; Špano, 2019; Špano and Duchan, 2021; Špano et al. 2022).

The shift in the determination of wave parameters on small, closed reservoirs concerns the wave spectrum (Michel, 1968) and wave field spectral characteristics (Mahmood et al., 2010; Vincent et al., 2002), which currently underpin designs and protection measures.

To simulate wave events generated with the aid of wind on water bodies, an appropriate mathematical model is required. The mathematical models that are presently used are primarily based on wave spectra which have been derived from measurements taken from the seas or oceans, i.e. water surfaces generally larger than those of ponds and the varied range of small water reservoirs typically found inland in the majority of states. For this reason, it seems appropriate to confirm the validity to small reservoirs of the aforementioned wave spectra measured on the open sea. Such research considers the “sea state”, which is the general condition of the free surface of the water body at a given location and point in time. A sea state wherein no increase in wave height is occurring is referred to as a fully developed sea (Marinet, 2015).

The first practical use of wind-wave forecasting dates back to the first half of the 20th century. In 1956, the U.S. National Weather Service used a numerical wave forecasting model for the first time. It only worked with fundamental values, which included wave height and period. The first spectral models did only consider waveform and energy increase spectra. This led to the creation of first and second-generation (1G and 2G) wave models (Marinet, 2015).

The group of 1G and 2G models comprises the Pierson-Moskowitz, Bretschneider, Ochi-Hubble, Torsethaugen, JONSWAP, and McCormick spectra (Alves et al., 2003; Bretschneider, 1959; Hasselmann et al., 1973; Klaus and Olbers, 1973; McCormick, 1998; Ochi and Hubble, 1976; Torsethaugen, 1993). The Pierson-Moskowitz spectrum considered Phillip's arguments (Phillips, 1958) and verified them against records measured inside the North Atlantic Ocean for a fully developed sea. The spectrum assumes that there are no waves in the sea that can spread on their own without being aided by the wind. The Pierson-Moskowitz spectrum is only dependent on 1 input parameter (Alves et al., 2003). The Bretschneider spectrum (SMB) is sea-derived. It is based on the Pierson-Moskowitz spectrum, but supplements it with parameters that can change the slenderness of the spectrum height. Bretschneider is an appropriate model for 'fully developed seas', i.e. water reservoirs in which the wind blows fetch lengths enough over a sufficiently open stretch of water body and waves with excessive frequency reach frequency equilibrium. In the part of the spectrum in which the frequency is greater than the height frequency ($\omega > \omega_p$), the power distribution is proportional to $\alpha^{-5}$. The Bretschneider spectrum can also be compared to the JONSWAP spectrum if the steepness factor is $\gamma = 1$ (Bretschneider, 1959). The last single peak spectrum is the McCormick spectrum, which replaces the existing spectra, whilst the Bretschneider and Pierson-Moskowitz spectrums no longer correspond to the measured spectrum. The spectra have been adjusted in shape so as to correspond more closely to the measured records (Yarde et al., 1996). The Pierson-Moskowitz and Bretschneider spectra cannot work with waves that propagate by themselves without the aid of the wind. Another spectrum used is the JONSWAP spectrum. It is based on measurements taken within the North Sea and considers the limited fetch length of the region wherein the wind impacts the water's surface. The JONSWAP spectrum is designed to show a very good shape with the effects of the power spectral density of wave events in small, closed reservoirs (Hasselmann et al., 1973; Klaus and Olbers, 1973).

Therefore, a two-peak spectrum has been developed wherein the primary height represents the frequencies of waves propagated by wind, and the second peak represents the frequencies of waves propagating without the aid of the wind. The first of these two-peak spectra is a six-dimensional wave spectrum that is created by combining 2 three-dimensional spectra. In English literature (Marinet, 2015) it is referred to according to the names of its 2 authors as the Ochi-Hubble spectrum, or simply as the two-peak spectrum. The spectrum is likewise valid for a 'developing sea', i.e. a water body wherein a rise in wave height continues to be occurring. The Ochi-Hubble spectrum input parameters were derived based on 800 sets of records measured within the North Atlantic Ocean (Ochi and Hubble, 1976). The Torsethaugen spectrum is another two-peak spectrum derived from measurements made within the Norwegian Sea and the North Sea (Torsethaugen, 1993).

The SWAMP (Surface Water Ambient Monitoring Program) study, in comparison to the 1G and 2G models, led to the decision that nonlinear interactions need to be additionally accounted for with the purpose of accommodating specific wind conditions. Consequently, in the 1980s this led to the creation of a third generation of wave models (3G) (Marinet, 2015). The third generation evolved in collaboration with Discrete Interaction Approximation (DIA) concerning nonlinear interactions. DIA is the idea behind the 3G wave model (WAve Model - WAM). There are presently numerous third-generation models, which include WAVEWATCH III, and SWAN. These models have now mostly replaced the first and second-generation models (Marinet, 2015).

The first 1G model was created by Sverdrup and Munk (1947), and was later improved by Bretschneider (1959). The Sverdrup, Munk, and Bretschneider (SMB) method combines a simple and direct concept of energy growth with empirical calibrations derived from field data. SMB has been used in the US Army's Shore Protection Manual since 1977 (US Army, 1977), and in the British Standard (BS-MS, 1993). Wilson (1955) formed parametric equations based on the SMB method and fitted them to new field data. In 1965, Wilson investigated developed equations and rearranged them for better accuracy in predicting wave height and period. Wilson´s method has been recommended by Japan's ports and harbor standards (Ocadij, 2002). Sibul (1955) also contributed to the development of new models for predicting wave heights and wave spectra for shallow water based on the parameters used by Sverdrup and Munk, so his work is considered a modification of the SMB solution. Saville et al. (1962) developed a method of estimating the maximum wave height that is likely to occur during the lifetime of the dam, as well as the corresponding wave period. This information is then used, along with other factors such as the maximum water level and safety margin, to calculate the required freeboard for the dam. Donelan (1980) published spectral forms that used similarity theory to predict wave heights, periods and directions. The forms were developed based on extensive measurements conducted in Lake Ontario, Canada, which generated data concerning full wave energy, frequency, and direction spectra. The US Army Corps of Engineers published a revised Shore Protection Manual (SPM, 1984), which also included simplified equations derived from Hasselmann's (1976) parametric model for use in estimating wave parameters based on wind duration and fetch limitation. In 2006, the US Army Corps of Engineers proposed the Coastal Engineer Manual (CEM) method as a replacement for the SPM. Based on data collected in Schafer Lake from 2005 to 2008, the American Society of Agricultural and Biological Engineers (ASABE) modified the Shore Protection Manual (SPM, 1984) method for use in small reservoirs in the United States. The Hasselmann et al. (1973) JONSWAP method is widely used in post-Soviet countries (Krylov et al., 1976). In the Czech Republic, wave parameters and characteristics must be calculated in accordance with the Czech standard specification (CSN) 75 0255.

Smith (1991) proposed improved expressions for wave height and peak frequency that incorporated Donelan's concept of wave development in off-wind directions. By incorporating Donelan's concept, Smith's model was able to better predict wave height and peak frequency in shallow water conditions.

Recently, there has been a lack of description of wind wave measurements on small closed reservoirs. Yarde et al. (1996) took wave height measurements at Megget reservoir (a flooded area of 260 ha), as well as at Loch Glascarnoch, located in Scotland, using the Donelan/JONSWAP approach and the simplified Donelan/JONSWAP approach to deal with wave height. As Donelan recommends, the Donelan/JONSWAP approach was used for the calculation of wave run-up on the closed small reservoirs (Owen and Steele, 1988). The conclusion

from the measurement of wind waves in the Megget Reservoir stated that the SMB method provided the best agreement, but it significantly underestimated wave heights in Loch Glascarnoch. In Loch Glascarnoch, the modified Donelan method gave the best agreement, but this method significantly overestimated wave heights in Megget Reservoir. The analysis was performed for a wind speed in the range of 14–30 m/s (Owen and Steele, 1988).

The second published article dealing with the measurement and evaluation of waves on small, closed reservoirs was published by Ozeren and Wren (2009). He used the Shore Protection Manual (SPM, 1977) to evaluate and predict waves using a parameter model based on the JONSWAP spectrum. The equations based on the JONSWAP spectrum for the calculation of the wave height and period were subsequently regressed into a form for the calculation of the wave height based on the evaluation of the measured data (wave heights) (SPM, 1977).

Choi et al. (2018) modified the factor which eliminated the boundary fetch limit and wind duration time of the SMB forms (Sverdrup and Munk, 1947 and Bretschneider, 1959), Wilsons´s forms (Wilson, 1955), Simplified Donelan and JONSWAP forms (Wilson, 1965), Donelan spectral forms (Donelan, 1980), Shore Protection Manual forms (SPM, 1984), the CEM forms (Vincent et al., 2002), and Wilson´s revised forms (Wilson, 1965), for the use of these forms for normal cyclone fetch lengths.

Kazeminezhad et al. (2005) investigated the ANFIS model for forecasting wave characteristics under fetch-limited conditions. For this purpose, a Lake Ontario data set from 2002 (NDBC, 2022) was utilized as training data, while a Lake Ontario data set from 2003 was used as testing data to evaluate the ANFIS models as well as the CEM technique. The result showed that in the analysed situation, the CEM technique over-predicts significant wave heights while under-predicting wave periods, and that both significant wave heights and wave periods are underestimated with the ANFIS models. However, it is possible to conclude that the accuracy of the ANFIS model is better than that of the CEM model.

Etemad-Shahidi et al. (2009) compared the SMB, Wilson's revised and CEM methods for wave height prediction from a Lake Ontario dataset, 2004. The SMB and Wilson´s revised methods showed very similar results. A comparison of the estimated models (SMB, WIL, CEM) under all scenarios reveals that the SMB approach is more effective than the others in general. The CEM method performed the worst, and for this method, they adjusted the equation by fitting it to the measured data for Lake Ontario.

All the studies, after measuring the wave heights on closed reservoirs, then use the equations of the parametric model based on the JONSWAP spectrum. This paper focuses on the determination of the spectral density of waves belonging to small closed reservoirs. It verifies its form with theoretical spectral densities. to confirm whether JONSWAP or any other model is suitable for use to determine the spectral density of waves.

## 2 METHODS

### 2.1 Theoretical considerations

The use of third-generation models involves the assumption that the wave run-out on small, closed reservoirs isn't efficiency due to time consuming and computing power (Mahmood et al., 2010). For this reason, this paper is concerned with evaluating the aforementioned 1G models and verifying their use for small reservoirs. It is common to use measurements and evaluations at higher wind speeds of 10 – 30 m/s, but in this case the speed range is up to 10 m/s and the wave height up to 15 cm.

*Spectral density of oscillatory wind waves*

Spectral power density, or the power transmitted by a wave, is the most important characteristic of a signal in the frequency domain. The spectrum of a signal can be viewed as a function that tells us what portion of the power is carried by what frequency components – it is a function of the spectral power density. The total power carried by the signal is calculated as the integral of the spectral power density from –∞ to +∞ (WAFO GROUP, 2017). The power spectrum $S$ is given by (Stoica and Moses, 2005):

$$S = \frac{a_i^2 + b_i^2}{2\Delta\omega} \tag{1}$$

where $a_i$ and $b_i$ are the $i$th elements of the vector $a$ and $b$, and $\Delta\omega$ is the sampling interval in the frequency domain, i.e. $\omega_i = i\Delta\omega$. The two-column matrix $S(\omega_i) = (\omega_i, S_i)$ is called the power spectrum $x(t)$. A sequence $\theta_i$ such that:

$$\cos\theta_i = \frac{a_i}{\sqrt{2S_i\Delta\omega}} \tag{2}$$

and

$$\sin\theta_i = \frac{b_i}{\sqrt{2S_i\Delta\omega}} \tag{3}$$

is called a phase sequence. The Fourier series is then written as follows (Stoica and Moses, 2005):

$$x(t) \approx m + \sum_{i=1}^{N} \sqrt{2S_i\Delta\omega}\cos(\omega_i t + \theta_i) \tag{4}$$

Since wind is irregular, it produces waves with irregular heights and periods. A deterministic approach cannot be used to describe the reservoir water surface due to that very same irregularity, which results in a constantly varying reservoir water surface. As opposed to typical wave periods and wavelengths, the statistical properties of that surface, such as average wave height, wave period, and wave direction, appear to vary slowly over time. The surface elevation of a wave can be viewed as the sum of numerous harmonic waves, each generated by turbulent wind at a different location and time. Since they have different origins, they are statistically independent. They travel across the reservoir independently, according to linear wave theory. Under these conditions and on a time scale of hundreds of characteristic wave periods, the reservoir surface elevation may be adequately characterized as a stationary, Gaussian process. Spectral density equations for wind waves were developed by Bretschneider (1959) in the form:

$$S(\omega) = p\omega^{-5}\exp(-q\omega^{-4}) \tag{5}$$

where $S(\omega)$ is the frequency spectrum of the water surface displacements at a fixed location corresponding to radial displacements, $p$ and $q$, depending on the wind field. Similarity analysis has been extensively applied to correlate wave spectra with generation factors. An example of one of the many ways to measure the similarity between wind wave spectra is by normalizing them as follows:

$$S(\omega)\omega_m/\sigma^2 = f(\omega/\omega_m) \tag{6}$$

where $\omega_m$ is the frequency at which $S(\omega)$ is maximum, $f(\omega/\omega_m)$ is a dimensionless function that is universal for the spectrum wave energy, and $\sigma^2$ is the variance of the water surface displacements, which is related to the spectral function as:

$$\sigma^2 = \int_0^\infty S(\omega)\, d\omega \quad (7)$$

*Empirical equations for the prediction of oscillatory wind waves*

Most of the empirical models (Bretschneider, 1959; Carter, 1982; CSN 750255, 1987; Donelan, 1980; Wilson, 1955; Wilson, 1965) for deepwater wave predictions are made using a parametric model based on the JONSWAP spectrum. JONSWAP is a wave energy spectrum generated from numerous marine wave data sets for fetch-limited, deepwater conditions. Based on wind speed, fetch, and duration, these methods yield the significant wave height $H_{m0}$ and peak period $T$ in the form:

$$H_{m0}, T = f(u_x, F, t, h) \quad (8)$$

where $u_x$ represents wind speed: $u_{10}$ is wind speed 10 m above the water level or terrain [m/s] or wind friction velocity $u_*$ [m/s] or wind stress factor $u_A$ [m/s]. A deepwater wave has a depth $h$ greater than half of its wavelength, which is the subject of interest. A wave travels the fetch length $F$ in the minimum duration $t$. Whenever the wind duration is less than the minimum duration $t$, the waves are said to be duration-limited waves. Once this threshold has been reached, the waves are defined as fetch-limited (Ozeren and Wren, 2009). Taking into account these assumptions, it is possible to eliminate the depth and duration time from the equation. The fetch-limited condition is then reduced to:

$$H_{m0}, T = f(u_x, F) \quad (9)$$

Empirical prediction relies on universal laws to govern relations among dimensionless wave parameters. Perhaps the most fundamental of these laws is the fetch-growth law. With constant winds and directions, waves will reach a stationary fetch-limited state of development over a fixed fetch. The wave heights will remain constant (in a statistical sense) through time, but they will vary along the fetch. Dimensionless wave height can be expressed as follows (Vincent et al., 2002):

$$\widehat{h_c} = \frac{g\widehat{H_{m0}}}{u_{10}^2} \quad (10)$$

where $\widehat{H_{m0}}$ is characteristic wave height [m], $u_{10}$ is wind speed 10 m above the water level or terrain [m/s] [m/s], $g$ is gravitational acceleration [m/s$^2$] and dimensionless fetch $\hat{F}$ is defined as:

$$\hat{F} = \frac{gF}{u_{10}^2} \quad (11)$$

where $F$ is a straight line distance over which the wind blows [m].

Fetch-limited wave heights are expected to correspond to the following formula:

$$\widehat{H_{m0}} = \lambda_1 \hat{F}^{m_1} \quad (12)$$

where $\lambda_1$ and $m_1$ are empirical coefficients [–].

Dimensionless wave frequency (defined simply as one over the spectral peak wave period) is defined as:

$$\widehat{f_p} = \frac{u_{10} f_p}{g} \quad (13)$$

where $f_p$ = the frequency of the spectral peak [W/Hz].

The existence of a stationary wave field also implies a fixed relationship between wave frequency and fetch in the form:

$$\widehat{f_p} = \lambda_2 \hat{F}^{m_2} \quad (14)$$

where $\lambda_2$ and $m_2$ are empirical coefficients [–].

Dimensional analysis of the basic wave generation relationship for fetch-limited conditions yields:

$$\frac{gH_{m0}}{u_x^\alpha}, \frac{gT}{u_x^\alpha} = f\left(\frac{gF}{u_x^\alpha}\right) \quad (15)$$

where $\alpha$ is an exponential coefficient [–] and $u_x$ represents wind 10 m above the water level, or wind friction velocity, or wind stress factor [m/s].

The wind speed, duration, direction, and fetch all affect the height, period, and direction of the waves that are produced. Most of the time, either the duration or fetch is largely irrelevant. For instance, even a brief storm might result in high wave heights in an inland reservoir. Any increase in wind duration will not result in further wave growth because of the short fetch lengths. As a result, these waves are said to be fetch-limited. Fetch is described as a zone with relatively steady wind speed and direction. Fetch should be designed so that variances in wind direction and speed do not exceed 15 degrees and 2.5 metres per second (5.0 knots) from the mean wind speed. The fetch is always limited by the shoreline upwind from the point of interest (Vincent et al., 2002).

The models for the prediction of wave parameters in fetch-limited deep-water conditions contain three input variables: depth $H$ [m], fetch length $L$ [m], and wind speed at 10 m above the water level $u_{10}$ [m/s], or its modification. Data from anemometers were used to determine wave events for the purposes of this research. From the measured wind data, the wind direction and wind speed at the point of wave occurrence 10 m above the water surface needed to be determined first. The measuring device itself contained an anemometer that was located approximately 3.5 m above the water surface. To convert the velocity from the measurement at $z$ meters above the surface to 10 m above the surface, the SPM recommends (SPM, 1984):

$$u_{10} = u_z \left(\frac{10}{z}\right)^{1/7} \quad (16)$$

where $u_z$ is the wind speed measured $z$ meters above the surface [m/s], and $z$ is the height of the anemometers above the surface [m]. The most important calculated characteristics for the design of shoreline protection measures are wave height $h_c$ [m] and wave period $T$ [s].

Different average periods may be helpful when dealing with wave occurrence in water reservoirs of varying sizes. In small lakes and reservoirs or riverine settings, a 1 to 5 min wind duration is necessary to establish the maximum height at a fetch-limited state (Vincent et al., 2002).

### 2.2 Field measurements

For the long-term recording of oscillatory wind waves, the best choice is a closed small reservoir in which there's no significant variation in the water level and waves are generated ideally only by the wind. For the selected purposes, cooperation with the company Gravel sandpit Hulín was arranged. The measurements were taken at a relatively new reservoir created by still-ongoing sand and gravel mining. The reservoir is situated in Moravia, within the Zlín Region, in the district of Kroměříž, on the outskirts of the town of Hulín approximately 17 km south of Přerov and 25 km northwest of the city of Zlín in the Czech Republic (Figure 1). The small, closed reservoir is free of any

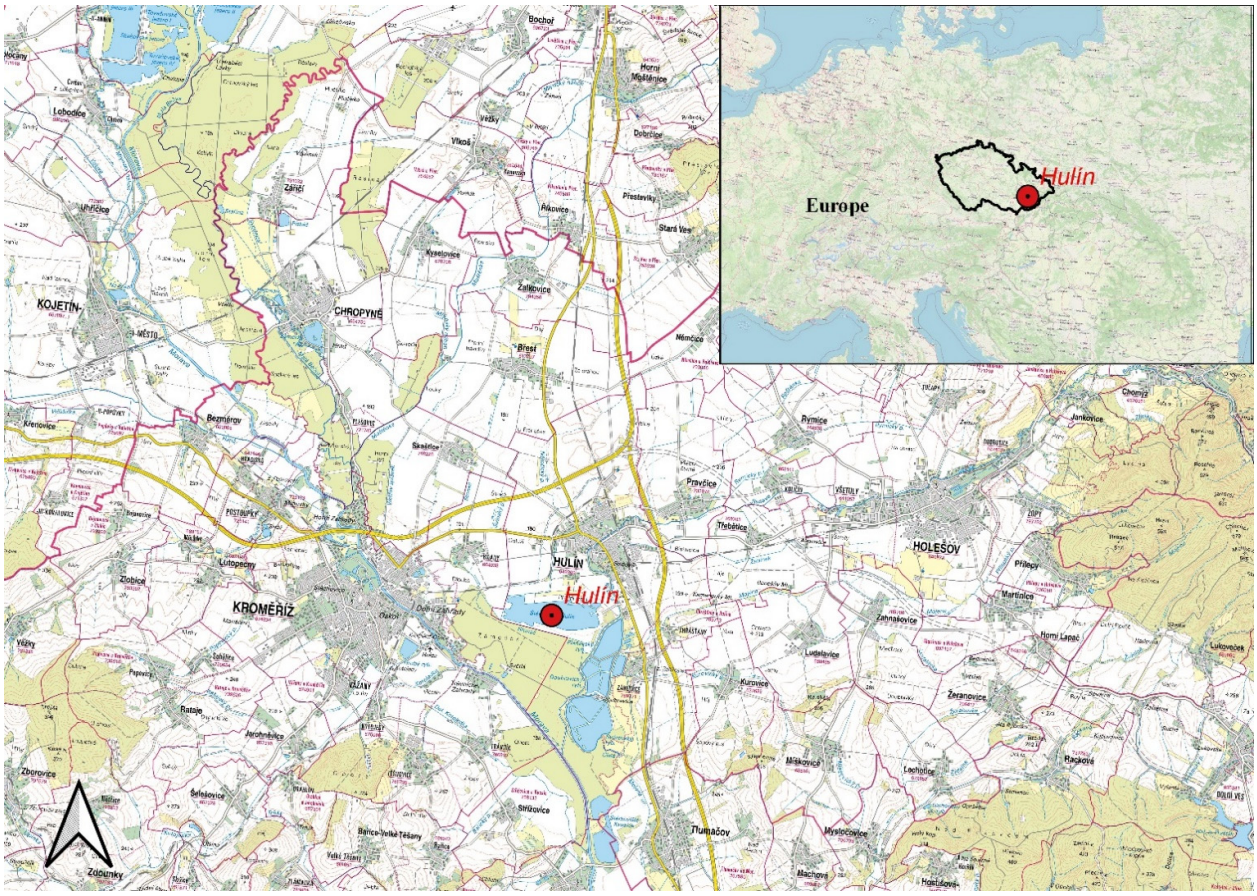



**Fig. 1.** Location of the area.

inflow and outflow that is subsidized from groundwater and rainfall. Thus, it is characterized by relatively regular water levels throughout the year. The flooded area of the small, closed reservoir is presently approximately 95 ha, and the area and volume of the reservoir are gradually increasing as the mining continues.

The measurements were taken at the flooded Hulín closed reservoir, where only wind-generated oscillating waves are formed. Since the reservoir is used for the extraction of sandy material, there is an average of 32 watergoing vessel movements per day. Waves produced by vessels may adversely affect the measurement of waves. This fact was taken into consideration. The decision on the location of the platform was aided by a 3D digital model of the morphology of the bottom of the reservoir taken from a vessel using a GSS station and a sonar (Špano et al., 2020). The resulting location of the platform was selected at the southeast bank of the reservoir (Figure 2).

The collection of data on the water level in the reservoir took place 6 times per second. The data were measured using three ultrasonic sensors that were fixed to the aforementioned platform. The exact location of the sensors within the X, Y, and Z coordinates was verified geodetically.

The platform supporting the measuring device was firmly attached to the bottom of the reservoir. The device for measuring and transmitting data on wind oscillation waves in water reservoirs consists of a sensor array (1) for sensing changes in the height level of the water surface, an anemometer that measures and stores wind direction and speed (4), an external antenna (8), a battery (9), a solar panel (10) and a set of elements located in a wiring box (13), namely a central control unit (3), to which the following elements are connected in turn: a microcontroller (2), a power regulator (11) and a voltage converter (12), a modem (7) and a communication unit (5) (Raspberry Pi) for collecting data from ultrasonic sensors, and the anemometer (Pelikán et al., 2020). A USB camera (6) was used for visual inspection of the system (Figures 3 and 4). The mentioned ultrasonic sensors scan the levels of the floats, which are fixed using taut cables so that they are not able to move horizontally, but only in the vertical plane (Figures 5 and 6).

There were occasional sensor failures during the measurements, and so for certain wave events only two or even only one sensor recorded the measured parameters of the waves. Communication between the communication device and the PC occurred via remote transmission using a SIM card and mobile internet. Remote device control (Teamviewer) was used to operate the equipment.

The uncertainties associated with wave height measurements may arise from variations in surface elevation, instrument calibration, and the accuracy of measurements in extreme wave conditions. The accuracy of the surface elevation measurements is 1 mm, and the time measurement accuracy is 1 ms. However, we expect the uncertainty of the wave height measurement to be around 1 cm, which is up to 10% of the heights recorded during the selected wave events. Similarly, uncertainties in wind speed measurements may be influenced by wind direction, instrument location, and the presence of obstructions in the measurement area. The accuracy of the wind velocity measurement is 0.1 m/s, and it is 22.5° for wind direction. Again, the uncertainty of the measurements should not exceed 10% of measured values.

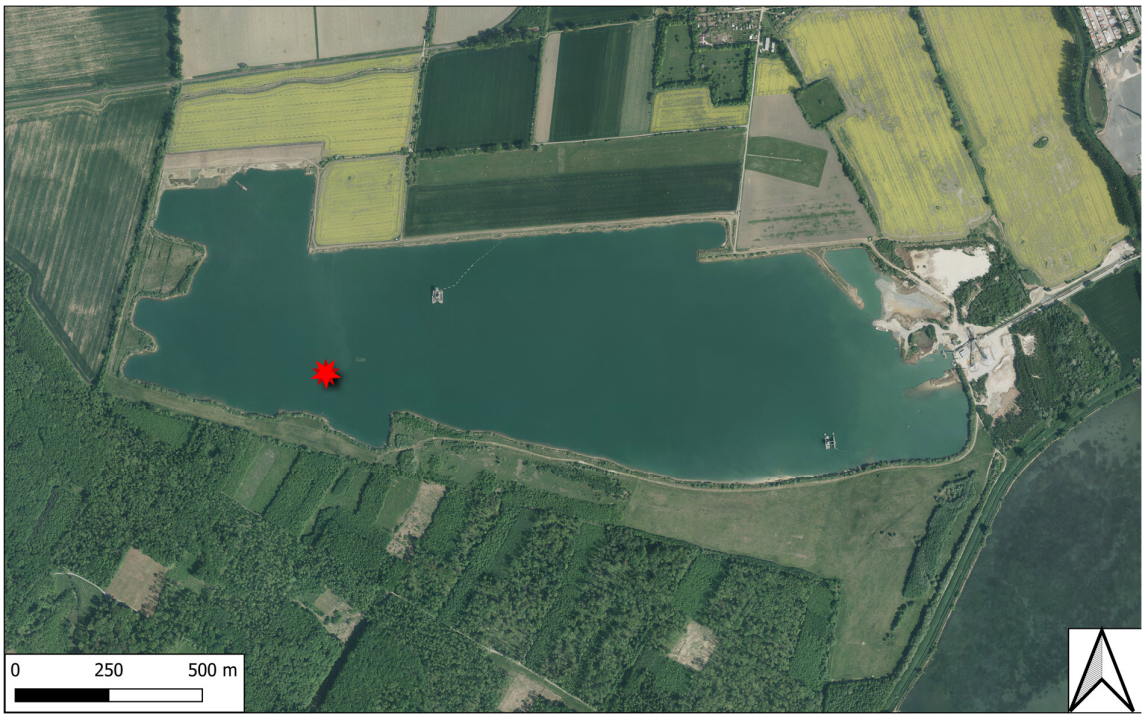



**Fig. 2.** Location of the platform and measuring device close to the most stressed bank of the reservoir (red star).

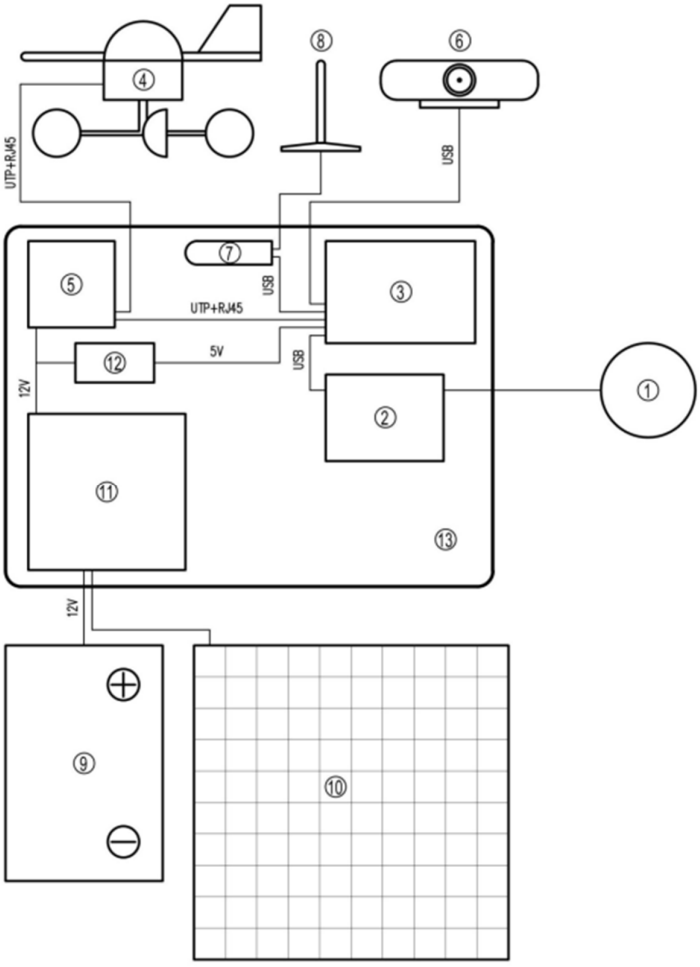



**Fig. 3.** Diagram of a device for measuring and transmitting data on wind oscillation waves on water reservoirs.

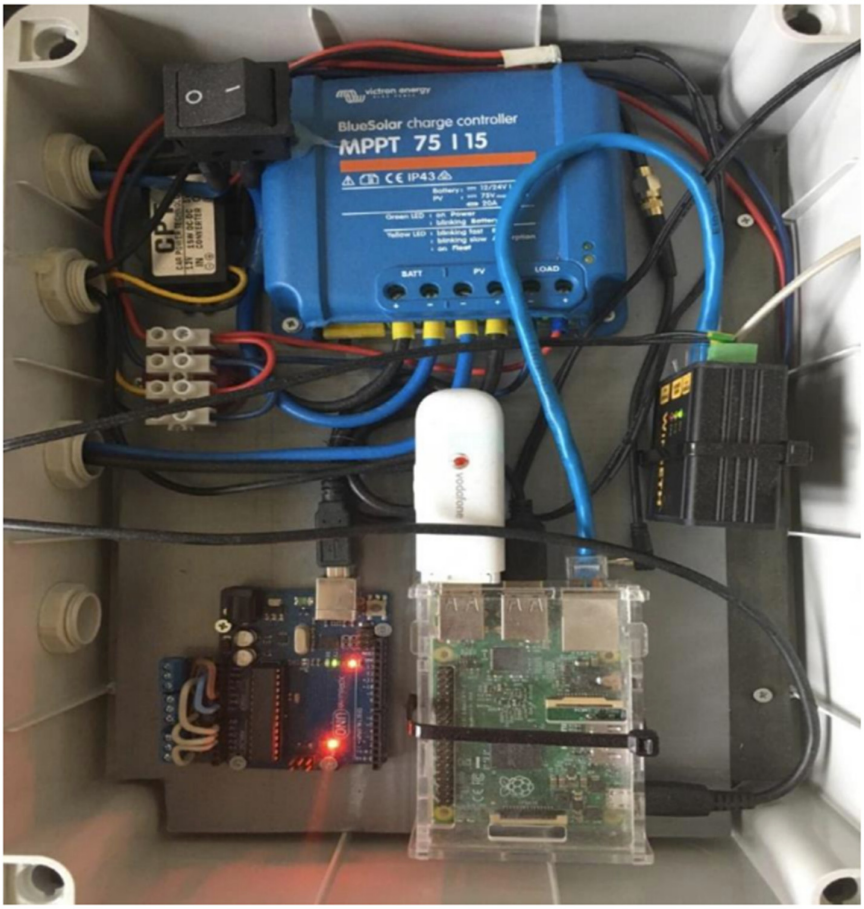



**Fig. 4.** Device for measuring and transmitting data on wind oscillation waves.

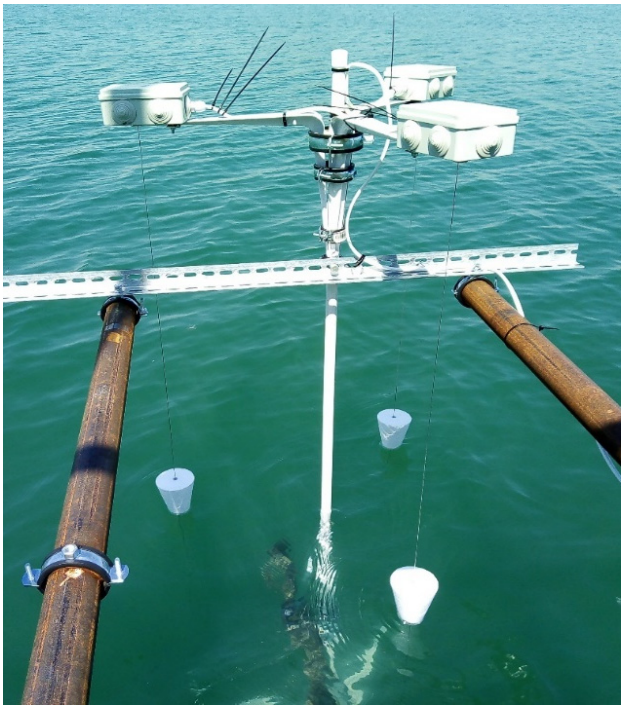


**Fig. 5.** View of ultrasonic level sensors and floats.

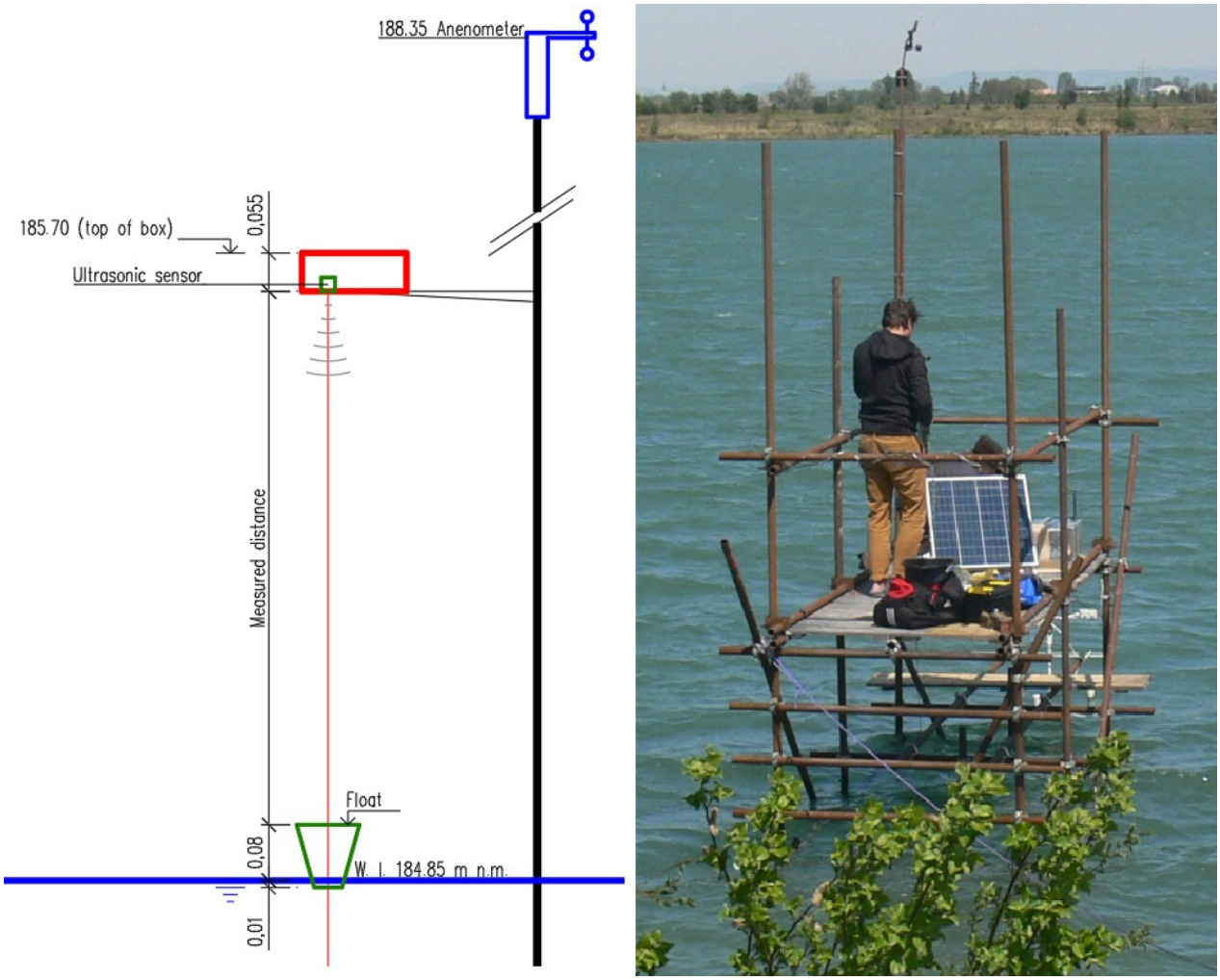



**Fig. 6.** Design of the measuring device (left) and the construction of the platform and measuring device (right).

The estimation of fetch length is also subject to uncertainty, and this can affect the accuracy of wave height and period predictions based on empirical formulas. For example, if the wind direction changes frequently or if the wind speed is highly variable, it can be difficult to accurately determine the fetch length for a given wave forecast. The fetch length was determined based on a digital terrain model (DTM) with an accuracy that is quite high (up to 1m). However, due to the ongoing mining activity, the uncertainty changes with the wind direction. It does not exceed 50 m out of around 1,000 m of fetch length, however, so the uncertainty of the fetch length can be estimated as being up to 5%. Steps were taken to minimize these uncertainties, such as ensuring proper instrument calibration and carefully selecting the measurement location. Nevertheless, it is important to acknowledge these potential sources of error in our collected data.

### 2.3 Identification of spectral density and wave parameters at the closed reservoir

The identification of wave events was performed using MATLAB software (MATLAB, 2022) using the WAFO toolbox, which was developed by Lund University (Brodtkorb et al., 2000; WAFO GROUP, 2017). The toolbox is used for statistical analysis and the simulation of random waves. It contains a comprehensive package of statistical tools for random wave analysis. Furthermore, statistical analyses of random processes are included in the program, with high accuracy, including simulation of any spectrum of Gaussian or transformed Gaussian waves divided into wave characteristics such as wave period or wave curve. The most commonly used spectra based on long-term measurements at sea level used in WAFO are listed in Table 1. WAFO was used to evaluate wave event data recorded in 2021.

Empirical relationships are often used to predict wave height and period. The most commonly used empirical models for the prediction of wave parameters in fetch-limited deep-water conditions are listed in Table 2.

## 3 RESULTS AND DISCUSSION

The first step in evaluating the data was to identify wave events. A wave event is understood to be a continuous segment of data that contains at least 1,000 waves, has a duration of at least 5 minutes, and produces an average wave height of more than 3 cm over the entire measurement period. The evaluation of wave events was carried out on data recorded in 2021 and shown in Table 3.

The measured wave heights were plotted on a graph (Le Méhauté, 1976) (Figure 7) to confirm the occurrence of deep-water wave conditions.

**Table 1.** Most commonly used spectra based on long-term measurements at sea level.

| Spectrum type | Spectrum equation | Eq. | Ref. |
|---|---|---|---|
| **Pierson–Moskowitz** | $S^+(\omega) = 5\frac{H_{m0}^2}{\omega_p\left(\frac{\omega}{\omega_p}\right)^5} exp\left(-\frac{5}{4}\left(\frac{\omega}{\omega_p}\right)^{-4}\right)$ | (17) | (Vincent et al., 2002) |
| **Bretschneider** | $S^+(\omega) = \frac{\left(\frac{H_{m0}}{4}\right)^2}{\omega_p} G_0 \left(\frac{\omega_p}{\omega}\right)^{-N} \exp\left(-\frac{N}{M\left(\frac{\omega_p}{\omega}\right)^M}\right)$ | (18) | (Bretschneider, 1959) |
| **JONSWAP** | $S^+(\omega) = \frac{\alpha g^2}{\omega^M}\exp\left(-\frac{M}{N}\left(\frac{\omega_p}{\omega}\right)^N\right)\gamma^{exp\left(\frac{-(\frac{\omega}{\omega_p}-1)^2}{2\sigma^2}\right)}$ | (19) | (Alves et al., 2003; Marinet, 2015) |
| **McCormick** | $S^+(\omega) = (M+1)\frac{\left(\frac{H_{m0}}{4}\right)^2}{\omega_p(\frac{\omega_p}{\omega})^{M+1}}\exp\left(-\frac{(M+1)}{M(\frac{\omega_p}{\omega})^M}\right)$ | (20) | (McCormic, 1998) |
| **Ochi-Hubble** | $S^+(\omega) = \frac{1}{4}\sum_{i=1}^{2}\frac{\left(\left(\lambda_i+\frac{1}{4}\right)\omega_{p,i}^4\right)^{\lambda_i}}{\Gamma(\lambda_i)}\frac{H_{m0,i}^2}{\omega^{4\lambda_i}+1} exp\left(\frac{-\left(\lambda_i+\frac{1}{4}\right)\omega_{p,i}^4}{\omega^4}\right)$ | (21) | (Ochi and Hubble, 1976) |
| **Torsethaugen** | $\int_0^\infty S^+(\omega;\, H_{m0,i}, \omega_{p,i}, \Upsilon_i, N_i, M_i, \alpha_i)d\omega = \frac{H_{m0,i}^2}{16}$, | (22) | (Torsethaugen, 1993) |

**Note**: $H_{m0}$ is the characteristic wave height [m], $\omega_p$ is the peak angular frequency [rad/s], $\omega$ is the angular frequency [rad/s], $G_0$ is the normalization factor of the Bretschneider function [–], $N$ is the scalar defining the height of the peak spectrum [–], $M$ is the parameter determining the width of the spectrum [–], $\alpha$ is the normalization constant of the JONSWAP spectrum [–], parameter $\sigma = 0.07$ [–] for values of $\omega$ less than $\omega_p$, otherwise $\sigma = 0.09$ [–], parameter $M = 5$ [–] and $N = 4$ [–], $\gamma$ is a peak parameter that takes values from 1 to 7 [–], $M$ is the empirical coefficient in the McCormick spectrum [–], index $i = 1$ denotes the low-frequency element of the wave event, index $i = 2$ denotes the high-frequency element of the wave event, $\lambda_i$ is the shape parameter of the Ochi-Hubble spectrum [-], and $\Gamma(\lambda_i)$ is a gamma function.

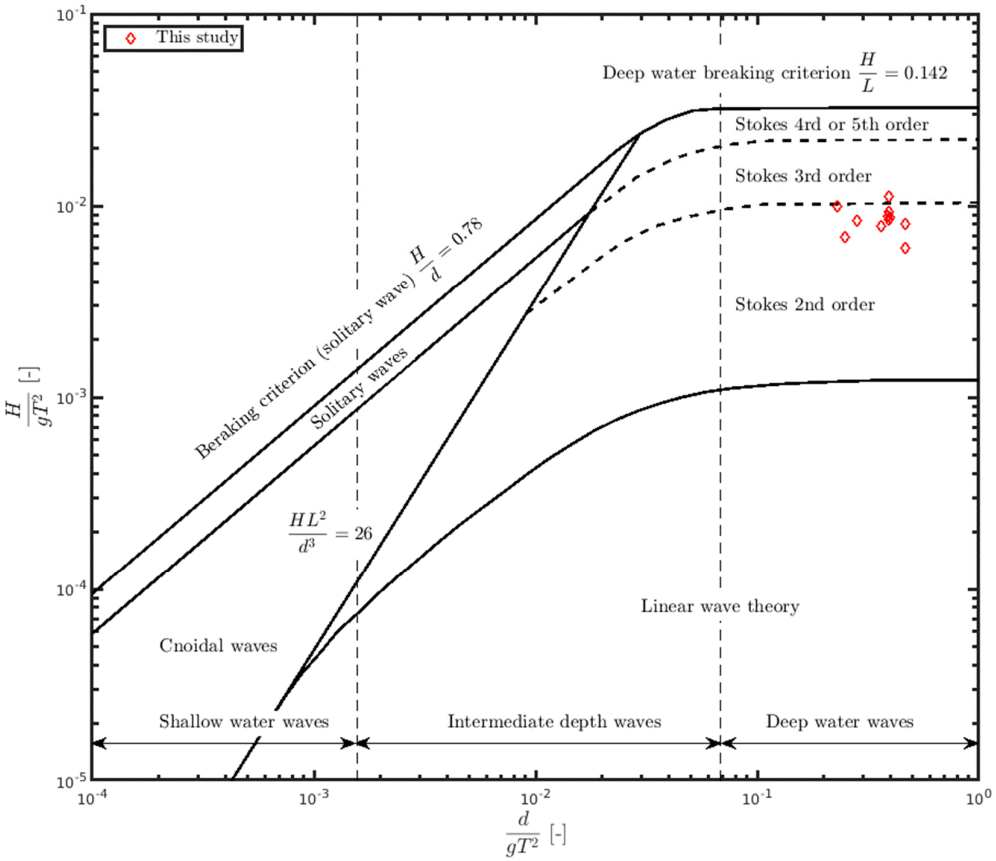



**Fig. 7.** The measured wave heights plotted to approximate the validity of wave propagation theories (red dots–this study, where $d$ is the depth of the water [m] and $L$ is the length of the waves [m]).

**Table 2.** Most commonly used empirical models for the prediction of wave parameters in fetch-limited deep-water conditions.

| Empirical approach | Significant wave height and period | Eq. | Ref. |
|---|---|---|---|
| **Sverdrup, Munk and Bretschneider method (SMB)** | $\frac{H_{m0}g}{{u_{10}}^2} = 0.283\tanh\left(0.0125\left(\frac{gF}{{u_{10}}^2}\right)^{0.42}\right)$<br>$\frac{Tg}{u_{10}} = 7.540\tanh\left(0.077\left(\frac{gF}{{u_{10}}^2}\right)^{0.25}\right)$ | (23, 24) | (Sverdrup and Munk,1947; Bretschneider,1959) |
| **Wilson's method (WIL)** | $\frac{H_{m0}g}{{u_{10}}^2} = 0.26\tanh\left(0.01\left(\frac{gF}{{u_{10}}^2}\right)^{0.5}\right)$<br>$\frac{Tg}{u_{10}} = 1.40\tanh\left(0.044\left(\frac{gF}{{u_{10}}^2}\right)^{0.33}\right)$ | (25, 26) | (Wilson,1955) |
| **Sibul (SIB)** | $\frac{H_{m0}g}{{u_{10}}^2} = 0.00323\left(\frac{gF}{{u_{10}}^2}\right)^{0.435}$ | (27) | (Sibul, 1955) |
| **Saville (SAV)** | $\frac{H_{m0}g}{{u_{10}}^2} = 0.0026\left(\frac{gF}{{u_{10}}^2}\right)^{0.47}$<br>$\frac{Tg}{u_{10}} = 0.45\left(\frac{gF}{{u_{10}}^2}\right)^{0.28}$ | (28, 29) | (Saville et al.,1962) |
| **Revisited Wilson's method (WIL revisited)** | $\frac{H_{m0}g}{{u_{10}}^2} = 0.30\left[1-\left[1+0.04\left(\frac{gF}{{u_{10}}^2}\right)^{0.5}\right]^{-2}\right]$<br>$\frac{Tg}{u_{10}} = 8.199\left[1-\left[1+0.08\left(\frac{gF}{{u_{10}}^2}\right)^{0.33}\right]^{-5}\right]$ | (30, 31) | (Wilson,1965) |
| **JONSWAP method (JON)** | $\frac{H_{m0}g}{{u_{10}}^2} = 0.00178\left(\frac{gF}{{u_{10}}^2}\right)^{0.5}$<br>$\frac{Tg}{u_{10}} = 0.352\left(\frac{gF}{{u_{10}}^2}\right)^{0.3}$ | (32, 33) | (Hasselman et al.,1973) |
| **Krylov (KRV)** | $\frac{H_{m0}g}{{u_{10}}^2} = 0.16\left\{1-\left[\frac{1}{1+0.006\left(\frac{gF}{{u_{10}}^2}\right)^{0.5}}\right]^2\right\}$ | (34) | (Krylov et al., 1976) |
| **Donelan method (DON)** | $\frac{H_{m0}g^{0.62}}{{u_{10}}^{1.24}} = 0.00366F^{0.38}$<br>$\frac{Tg^{0.77}}{{u_{10}}^{0.54}} = 0.46\frac{F^{0.23}}{1.85}$ | (35, 36) | (Donelan,1980) |
| **Shore Protection Manual (SPM)** | $u_A = 0.71{u_{10}}^{1.23}$<br>$\frac{H_{m0}g}{{u_A}^2} = 0.0016\left(\frac{gF}{{u_A}^2}\right)^{0.5}$<br>$\frac{Tg}{u_A} = 0.286\left(\frac{gF}{{u_A}^2}\right)^{0.33}$ | (37, 38, 39) | (SPM, 1984) |
| **Czech National Standard CSN 75 0255 (CSN)** | $\frac{H_{m0}g^{0.53}}{{u_{10}}^{1.06}} = 0.0026F^{0.47}$<br>$\frac{Tg^{0.72}}{{u_{10}}^{0.44}} = 0.46F^{0.28}$ | (40, 41) | (CSN 75 0255, 1988) |
| **Smith (SMT)** | $\frac{H_{m0}g}{{u_A}^2} = 0.0015\left(\frac{gF}{{u_A}^2}\right)^{0.5}$<br>$\frac{Tg}{u_A} = 0.3704\left(\frac{gF}{{u_A}^2}\right)^{0.28}$ | (42, 43) | (Smith, 1991) |
| **Coastal Engineer Manual (CEM)** | $u_* = \sqrt{0.001(1.1+0.035u_{10})}u_{10}$<br>$\frac{H_{m0}g}{{u_*}^2} = 0.0413\left(\frac{gF}{{u_*}^2}\right)^{0.5}$<br>$\frac{Tg}{u_*} = 0.651\left(\frac{gF}{{u_*}^2}\right)^{0.33}$ | (44, 45, 46) | (Vincent et al., 2002) |
| **Coastal Engineer Manual modified (CEM Modified)** | $\frac{H_{m0}g}{{u_*}^2} = 13.48\left(\frac{gF}{{u_*}^2}\right)^{0.1342}$ | (47) | (Etemad-Shahidi et al., 2009) |
| **Shore Protection Manual modified (SPM Modified)** | $\frac{H_{m0}g}{{u_A}^2} = 0.0025\left(\frac{gF}{{u_A}^2}\right)^{0.44}$<br>$\frac{Tg}{u_A} = 0.4147\left(\frac{gF}{{u_A}^2}\right)^{0.28}$ | (48, 49) | (Ozeren and Wren, 2009) |
| Note: To calculate the wave height and period in the shallow zone (with the influence of depth), it is necessary to use equations from the relevant literature. | | | |

**Table 3.** Recorded wave events and their basic characteristics–sensor 2–duration, period, height, and spectral density.

| Data set - Wave event | Duration | Mean period | Significant wave height | Type of spectral density* |
|---|---|---|---|---|
| | $t$ [min] | $T$ [s] | $H_{m0}$ [m] | $S^{+}(\omega)$ [m²s/rad] |
| **14/1/2021** | 570 | 0.8869 | 0.0866 | Pierson-Moskowitz (Bretschneider) |
| **4/2/2021** | 255 | 0.8820 | 0.0662 | Pierson-Moskowitz (Bretschneider) |
| **5/3/2021** | 180 | 0.8863 | 0.0719 | JONSWAP (Bretschneider) |
| **1/8/2021** | 360 | 0.8837 | 0.0655 | Pierson-Moskowitz (Bretschneider) |
| **2/8/2021** | 210 | 0.8832 | 0.0648 | Pierson-Moskowitz (Bretschneider) |
| **10/8/2021** | 60 | 1.1094 | 0.0834 | JONSWAP (Bretschneider) |
| **11/8/2021** | 540 | 0.8107 | 0.0386 | JONSWAP (Bretschneider) |
| **24/8/2021** | 360 | 1.1538 | 0.1297 | Pierson-Moskowitz (Bretschneider) |
| **25/8/2021** | 360 | 0.8131 | 0.0521 | McCormick (Bretschneider) |
| **29/8/2021** | 570 | 0.8911 | 0.0689 | Bretschneider |
| **17/9/2021** | 720 | 0.9192 | 0.0647 | Pierson-Moskowitz (Bretschneider) |
| **24/9/2021** | 660 | 1.0445 | 0.0899 | Pierson-Moskowitz (Bretschneider) |

*This is the shape of the spectrum that was matched most accurately in the implicit form. The spectrum in brackets corresponds most accurately mached spectrum when adjusting the coefficients $M$ in the range of values between 9.0 and 10.0 [–] and $N$ in the range of values 2.9 to 6.8 [–].

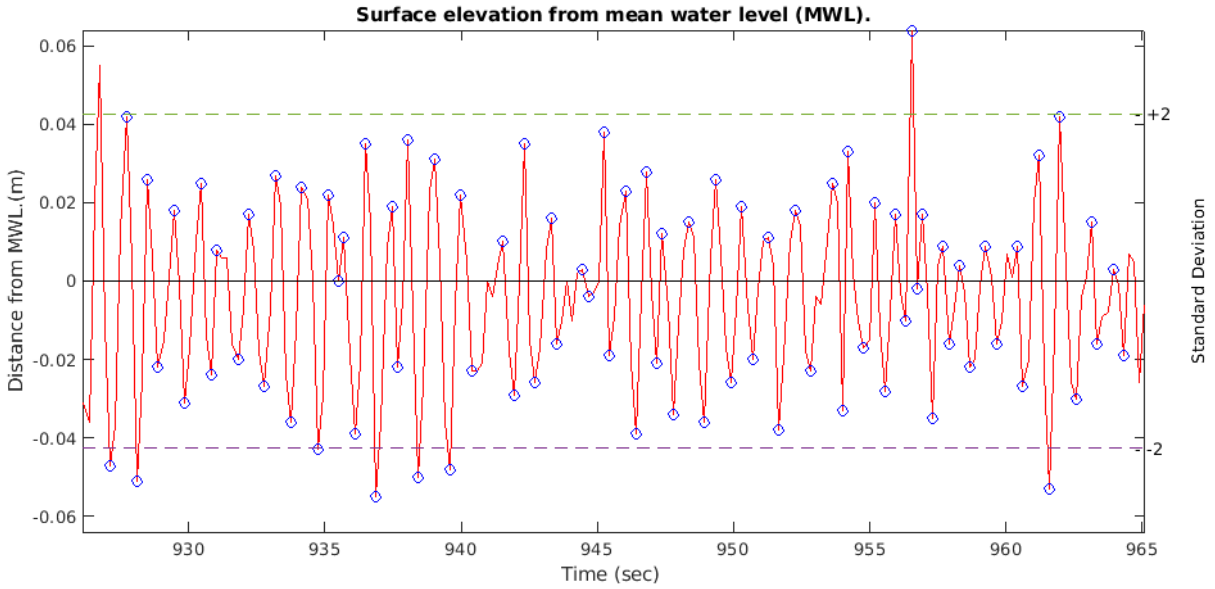



**Fig. 8.** Wave event – example of measured data.

At first, a complete set of 12 wave events was determined based on conditions mentioned at the beginning of this chapter (Figure 8). Using the WAFO toolbox, effects in the shape of the wave spectra were generated for each wave event. The results can be divided into 2 groups. The first group contains the power spectrum density (PSD) and the second set of results contains spectral densities. A comparison of the wave spectrum shapes from the two groups' results can then be made.

To choose the correct parameter model, data were processed from 12 wave events, during which a total of 39 wave measurements were made using 3 sensors from which spectral density waves were transmitted. The WAFO toolbox enabled the generation of the spectral density $S(\omega)$ and its comparison with the empirical spectra generated during the wave events labelled $S^{+}(\omega)$. The toolbox includes the option to generate Pierson-Moskowitz, Bretschneider, JONSWAP, McCormick, Ochi-Hubble, and Torsethaugen spectra (WAFO GROUP, 2017). All the above spectra have been specified for each wave event to be generated and displayed graphically, along with spectral density $S(\omega)$ (Figure 9). The best shape match between the spectral density of $S(\omega)$ and the empirical spectra of $S^{+}(\omega)$ can then be determined from the graphs. Before the data evaluation, it was assumed that the best match would be found with the JONSWAP spectrum. This spectrum is suitable for sites where there are not 'fully developed seas' and where waves cannot spread without wind (Marinet, 2015). The small, closed reservoir by Hulín should have fulfilled these conditions (Pelikán et al., 2015). Therefore, 1G and 2G models (JONSWAP, Bretschneider, etc.) should be appropriate for modelling waves on small, closed reservoirs.

The Bretschneider spectrum was the best match after analysing the graphs of all the wave events. In general, the Bretschneider spectrum parameters fluctuated, for $N$ between 2.9 and 6.8, and for $M$ between 9.0 and 10.0. However, the Bretschneider spectrum (or any of the other empirical spectra tested) does not offer the correct $S^{+}(\omega)$ energy values for

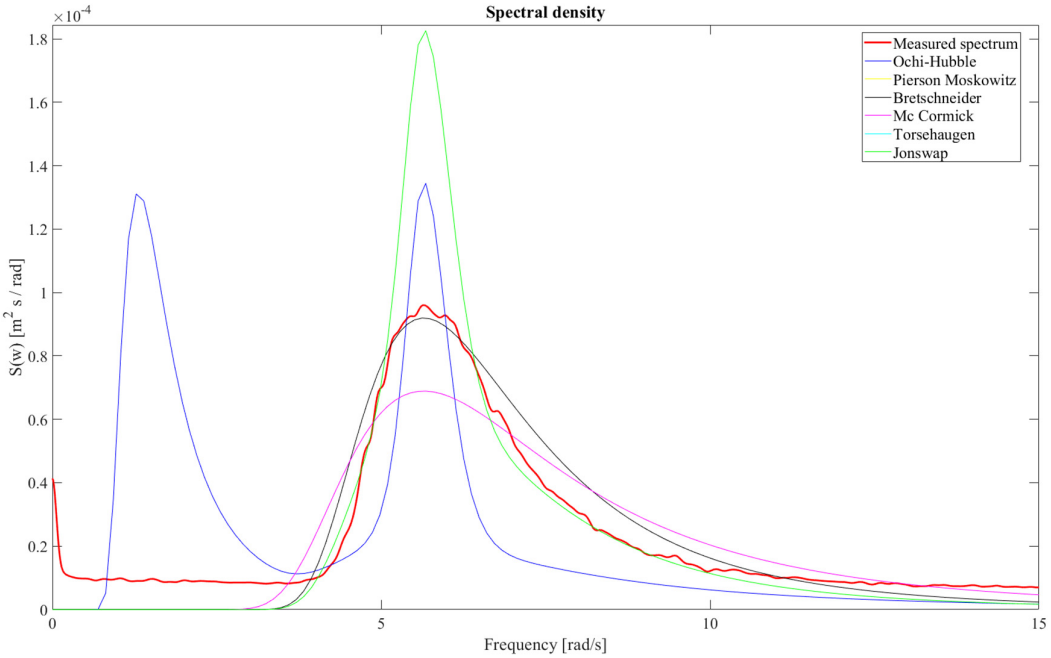



**Fig. 9.** Comparison of spectral density $S(\omega)$ (red) with empirical spectra $S^{+}(\omega)$ (blue (Ochi-Hubble), green (JONSWAP), purple (Mc Cormic), magenta (Torsehaugen) – in this case the same as JONSWAP, yellow (Pierson-Moskowitz) – in this case the same as JONSWAP, and black (Bretschneider)) - example of an evaluated spectrum.

low-frequency and low-altitude waves. From the result, it can be concluded that in the case of the Hulín closed reservoir at the most stressed bank on a running fetch, there can be no balance between high-frequency waves and a fully developed Bretschneider spectrum, but the Bretschneider spectrum was the closest of all the spectra to the measured spectrum. Therefore, to confirm the assumption of the occurrence of the Bretschneider spectrum on a closed small reservoir, it is advisable to calculate the wave height and period using the equations derived by Bretschneider (Bretschneider, 1959; Sverdrup and Munk,1947) and compare them with other empirical equations (Table 2) and measured wave heights (Table 3).

First, the fetch length $F$ associated with the reservoir shore location under study is considered to be the longest straight-line distance from the opposite bank of the water surface in the case of JONSWAP, Bretschneider (SMB), CSN 750255, and the Shore Protection Manual (SPM). Donelan provides an alternative definition of effective fetch by suggesting that fetch length should be measured along the wave direction rather than the wind direction. The Coastal Engineering Manual (CEM) suggests using straight-line fetches in calculations.

The SMB and SPM propose that the equivalent fetch should be estimated based on the narrow energy distribution in the wave spectrum. The average of the fetch lengths was recorded at 3° intervals over a range of 12° above and below the bearing of the average wind direction. CSN 75 0255 proposed the estimation of the mean value of fetch lengths recorded at 6° intervals over a range of 42° above and below the average wind direction. Since the models differ with regard to fetch determination, the simplest solution of assuming straight-line fetch in the most common wind direction has been adopted in this study.

The wave fetch length based on flow direction rasters was calculated in ArcGIS. For the analysis, raster plots over the range of the reservoir with a constant flow direction value (Figure 10) were created. Each of the directions has a raster value (1, 2, 4, 8, 16, 32, 64, 128). Using the raster values for a given direction, the run length is then calculated using the ArcGIS Flow length tool.

Figure 10 shows a raster for the southeast direction with the direction code = 2 and a maximum wind runout length of 939 m. Each pixel in this grid represents the distance from north-western boundary of the reservoir to the pixel position. Significant changes in pixel values indicate significant changes in distance from the reservoir boundary. The southeast direction already has a significant wind run-up (within +/– 45 degrees), and thus no correction is necessary for this part of the shore. The evaluation is performed for directions 0° (north), 45° (north-east), 90° (east), 135°(south-east), 180° (south), 225°(south-west), 270° (west), 315°, and 360° (north). The whole procedure was automated using zonal statistics tools, which determine the maximum run-up lengths for given parts of the shore and directions.

For each measured event, the relative frequency of wind was set in order to evaluate wind direction, wind speed, and the corresponding fetch length $F$ in the given direction (Table 4).

**Table 4.** Measured and evaluated data from measurements of wind speed and direction.

| Data set - Wave event | Number of wave events | Prevailing wind direction | Average wind speed 3.5 m above the water level $U_z$ [m/s] | Fetch length $F$ [m] |
|---|---|---|---|---|
| 14/1/2021 | 1 | SSW | 1.68 | 120 |
| 4/2/2021 | 2 | ESE | 2.46 | 700 |
| 5/3/2021 | 3 | NW | 2.81 | 200 |
| 1/8/2021 | 4 | W | 4.81 | 480 |
| 2/8/2021 | 5 | NE | 2.44 | 110 |
| 10/8/2021 | 6 | SSE | 4.42 | 120 |
| 11/8/2021 | 7 | WNW | 3.35 | 150 |
| 24/8/2021 | 8 | NE | 5.29 | 110 |
| 25/8/2021 | 9 | NNE | 2.22 | 220 |
| 29/8/2021 | 10 | NW | 3.90 | 120 |
| 17/9/2021 | 11 | WNW | 4.98 | 150 |
| 24/9/2021 | 12 | WNW | 7.64 | 150 |

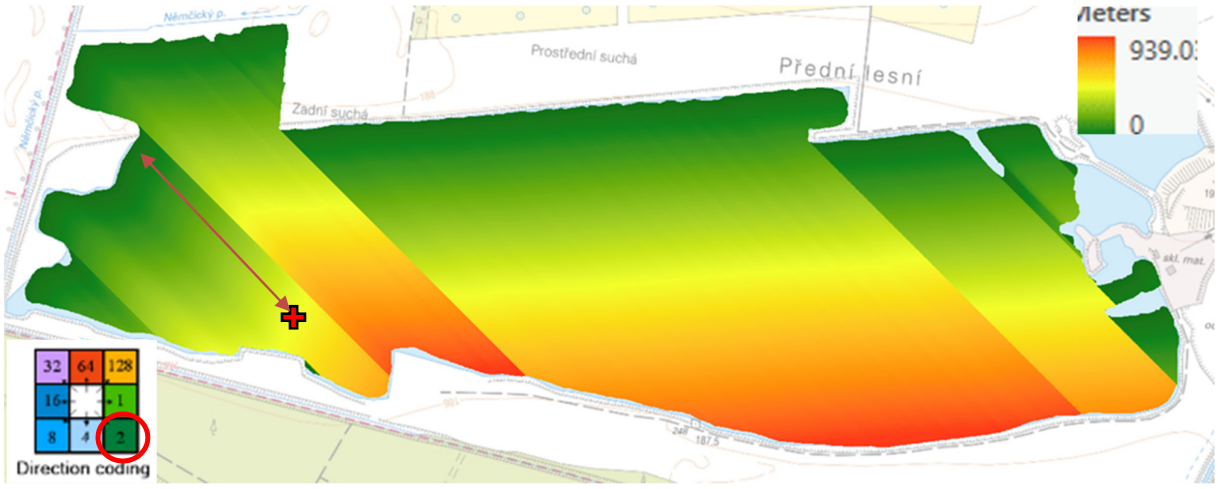



**Fig. 10.** Raster with fetch lengths for the southeast direction (direction code = 2; the length of the red line is the raster value at the red point).

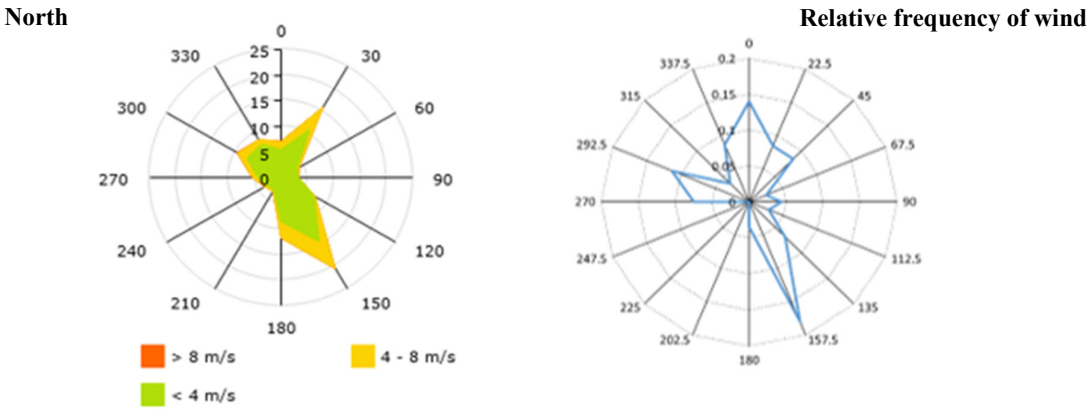



**Fig. 11.** Example of evaluation of wind data – wind rose (left: frequency and direction of the wind from radar (CAS, 2022), right: evaluated frequency and direction of the wind measured by anemometer).

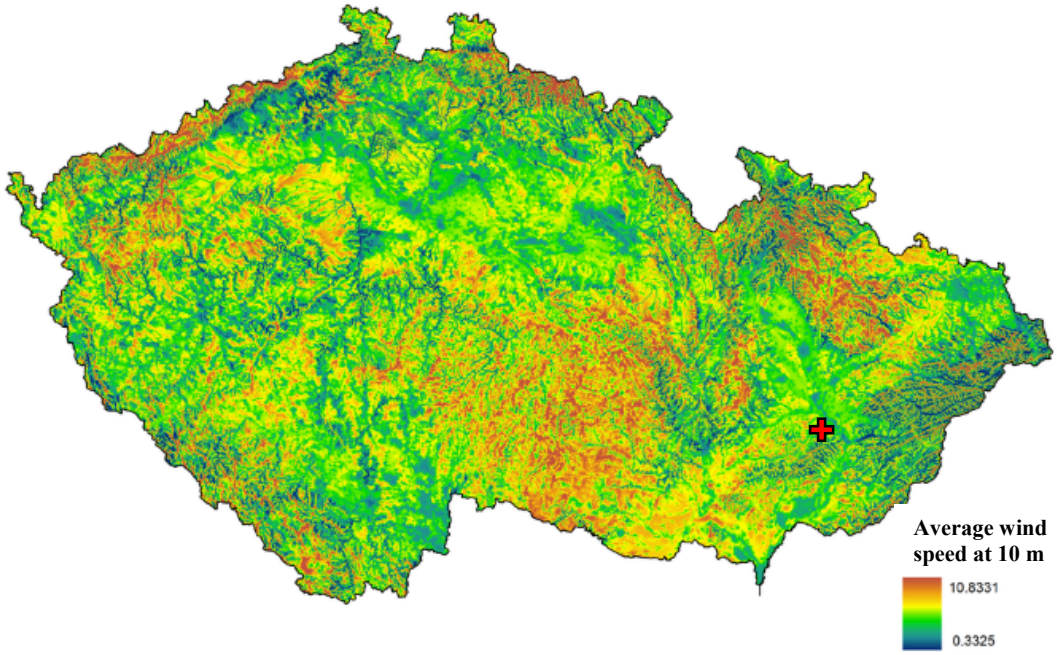



**Fig. 12.** Example of calculated average wind speed data at 10 m above ground for the Czech Republic (Hanslian et al., 2013).

To determine the most common waves, long-term measurements of wind events are required. Wind radar data and directions from wind roses can be used to determine maximum wind speeds for closed reservoirs.

From the measurements at the pilot site, it can be seen that the wave direction and wind direction indicated by the measured wind rose diagram are similar to the wind rose diagram from the radar data (CAS, 2022), as shown in Figure 11. It can be concluded that the directions and survey locations for measuring devices can be planned based on radar data. The rose direction shows that the average wind speed of the reservoir is as high as 8 m/s (Fig. 11 and Fig. 12). Therefore, the measurements (Table 4) cover the entire range of average winds occurring over the Hulín reservoir.

A total of 12 wave events were evaluated for which wind speeds, wind stress factors, wave heights, and wave periods were calculated (Table 5, Table 6, and Table 7; Figure 13, Figure 14, Figure 15, and Figure 16).

The best estimate of $H_{m0}$ is provided by the formulas of SMB, WIL, SIB and SAV, with an average underestimated RMSE = 0.017 m. Rather worse results are provided by the Wilson revisited Equation (30) from (Wilson, 1965), with an average underestimated RMSE = 0.30 m. The best estimation of $T$ is provided by the formula of SMB Equation (24) developed by (Bretschneider,1959; Sverdrup and Munk,1947) with an average underestimated RMSE = 0.062 s. Rather worse results are again provided by the Wilson revisited Equation (31) from (Wilson, 1965) with an average overestimated RMSE = 2.196 s. The significant

**Table 5.** The wind speed 10 m above the water level (Equation 7), and calculated wind speeds for different models (CEM, SPM).

| Data set - Wave event | Number of wave events | Wind speed 10 m above the water level $u_{10}$ [m/s] | Calculated wind stress factor $u_*$ [m/s] Eq. (33) | Calculated wind speed $u_A$ [m/s] Eq. (38) |
|---|---|---|---|---|
| **1/14/2021** | 1 | 2.00 | 0.07 | 1.66 |
| **2/4/2021** | 2 | 2.93 | 0.10 | 2.66 |
| **3/5/2021** | 3 | 3.34 | 0.12 | 3.13 |
| **8/1/2021** | 4 | 5.71 | 0.21 | 6.05 |
| **8/2/2021** | 5 | 2.89 | 0.10 | 2.62 |
| **8/10/2021** | 6 | 5.24 | 0.19 | 5.45 |
| **8/11/2021** | 7 | 3.98 | 0.14 | 3.88 |
| **8/24/2021** | 8 | 6.29 | 0.23 | 6.81 |
| **8/25/2021** | 9 | 2.64 | 0.09 | 2.34 |
| **8/29/2021** | 10 | 4.63 | 0.16 | 4.68 |
| **9/17/2021** | 11 | 5.92 | 0.21 | 6.32 |
| **9/24/2021** | 12 | 9.08 | 0.34 | 10.71 |

**Table 6.** Measured heights of wind waves and results of different models for predicting wave height.

| | Wave height $H_{m0}$ [m] | | | | | | | | | | | | | | |
|---|---|---|---|---|---|---|---|---|---|---|---|---|---|---|---|
| **Number of wave events** | **Measured** | **SMB** | **WIL** | **WIL revisited** | **JON** | **DON** | **SPM** | **CSN** | **CEM** | **CEM modified** | **SPM modified** | **KRV** | **SIB** | **SAV** | **SMT** |
| **1** | **0.087** | 0.051 | 0.060 | 0.11 | 0.18 | 0.040 | 0.041 | 0.062 | 0.044 | 0.051 | 0.037 | 0.085 | 0.057 | 0.062 | 0.039 |
| **2** | **0.066** | 0.050 | 0.055 | 0.20 | 0.13 | 0.041 | 0.036 | 0.053 | 0.035 | 0.086 | 0.037 | 0.043 | 0.052 | 0.053 | 0.034 |
| **3** | **0.072** | 0.055 | 0.059 | 0.25 | 0.16 | 0.045 | 0.039 | 0.056 | 0.038 | 0.106 | 0.042 | 0.036 | 0.056 | 0.056 | 0.037 |
| **4** | **0.066** | 0.066 | 0.059 | 0.42 | 0.26 | 0.058 | 0.044 | 0.059 | 0.038 | 0.246 | 0.054 | 0.014 | 0.064 | 0.059 | 0.041 |
| **5** | **0.065** | 0.055 | 0.062 | 0.21 | 0.14 | 0.044 | 0.040 | 0.058 | 0.040 | 0.087 | 0.041 | 0.048 | 0.057 | 0.058 | 0.038 |
| **6** | **0.083** | 0.081 | 0.079 | 0.46 | 0.32 | 0.069 | 0.057 | 0.077 | 0.051 | 0.232 | 0.066 | 0.021 | 0.080 | 0.077 | 0.054 |
| **7** | **0.039** | 0.035 | 0.032 | 0.22 | 0.10 | 0.030 | 0.022 | 0.032 | 0.020 | 0.118 | 0.026 | 0.015 | 0.034 | 0.032 | 0.020 |
| **8** | **0.130** | 0.101 | 0.095 | 0.60 | 0.47 | 0.087 | 0.072 | 0.094 | 0.062 | 0.327 | 0.086 | 0.018 | 0.099 | 0.094 | 0.068 |
| **9** | **0.052** | 0.036 | 0.039 | 0.16 | 0.08 | 0.029 | 0.025 | 0.037 | 0.025 | 0.066 | 0.026 | 0.038 | 0.037 | 0.037 | 0.023 |
| **10** | **0.069** | 0.046 | 0.042 | 0.29 | 0.15 | 0.040 | 0.029 | 0.042 | 0.027 | 0.161 | 0.036 | 0.015 | 0.044 | 0.042 | 0.027 |
| **11** | **0.065** | 0.062 | 0.055 | 0.40 | 0.25 | 0.055 | 0.041 | 0.055 | 0.036 | 0.255 | 0.051 | 0.012 | 0.060 | 0.055 | 0.038 |
| **12** | **0.090** | 0.10 | 0.082 | 0.68 | 0.57 | 0.092 | 0.067 | 0.085 | 0.055 | 0.570 | 0.090 | 0.008 | 0.095 | 0.085 | 0.063 |

**Table 7.** Measured periods of wind waves and results of different models for predicting wave period.

| | Wave period $T$ [s] | | | | | | | | | | |
|---|---|---|---|---|---|---|---|---|---|---|---|
| **Number of wave events** | **Measured** | **SMB** | **WIL** | **WIL revisited** | **JON** | **DON** | **SPM** | **CSN** | **CEM** | **SPM modified** | **SAV** | **SMT** |
| **1** | **0.887** | 0.474 | 0.184 | 1.647 | 1.46 | 0.371 | 0.953 | 4.626 | 0.733 | 0.880 | 1.035 | 0.786 |
| **2** | **0.882** | 0.873 | 0.159 | 2.286 | 1.49 | 0.345 | 0.750 | 3.098 | 0.563 | 0.771 | 0.873 | 0.689 |
| **3** | **0.886** | 0.702 | 0.160 | 2.551 | 1.62 | 0.358 | 0.754 | 3.054 | 0.560 | 0.794 | 0.886 | 0.709 |
| **4** | **0.884** | 1.144 | 0.137 | 3.532 | 1.99 | 0.371 | 0.656 | 2.308 | 0.473 | 0.780 | 0.825 | 0.697 |
| **5** | **0.883** | 0.564 | 0.170 | 2.289 | 1.59 | 0.364 | 0.812 | 3.470 | 0.609 | 0.823 | 0.932 | 0.735 |
| **6** | **1.109** | 0.784 | 0.169 | 3.618 | 2.29 | 0.421 | 0.809 | 3.150 | 0.586 | 0.917 | 0.978 | 0.819 |
| **7** | **0.811** | 0.680 | 0.102 | 2.531 | 1.19 | 0.272 | 0.477 | 1.548 | 0.351 | 0.556 | 0.610 | 0.497 |
| **8** | **1.154** | 0.822 | 0.182 | 4.180 | 2.76 | 0.466 | 0.880 | 3.450 | 0.631 | 1.018 | 1.066 | 0.909 |
| **9** | **0.813** | 0.633 | 0.131 | 2.029 | 1.15 | 0.290 | 0.607 | 2.328 | 0.458 | 0.632 | 0.723 | 0.565 |
| **10** | **0.891** | 0.776 | 0.116 | 2.917 | 1.48 | 0.311 | 0.547 | 1.839 | 0.399 | 0.643 | 0.694 | 0.574 |
| **11** | **0.919** | 0.894 | 0.129 | 3.510 | 1.93 | 0.360 | 0.619 | 2.111 | 0.445 | 0.747 | 0.787 | 0.667 |
| **12** | **1.045** | 1.095 | 0.147 | 4.627 | 2.91 | 0.447 | 0.725 | 2.472 | 0.511 | 0.925 | 0.933 | 0.826 |

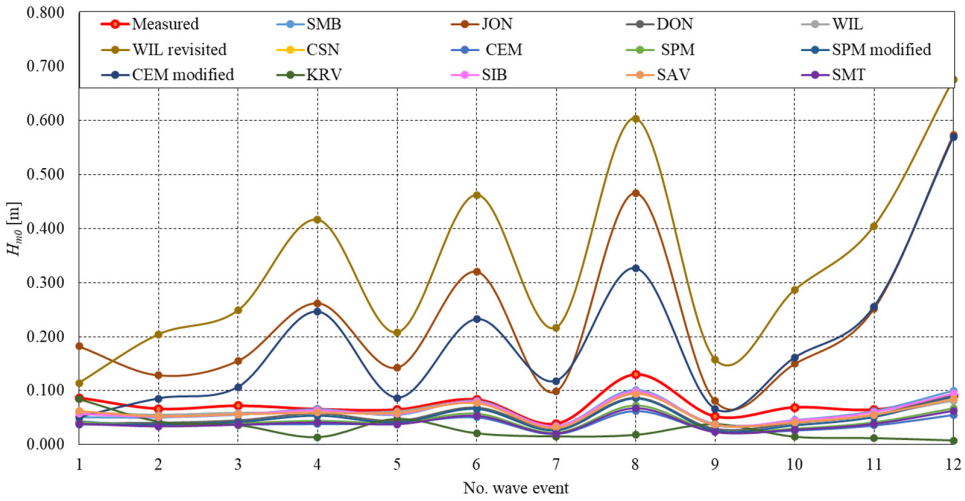



**Fig. 13.** Comparison of measured and calculated wave heights (Table 6).

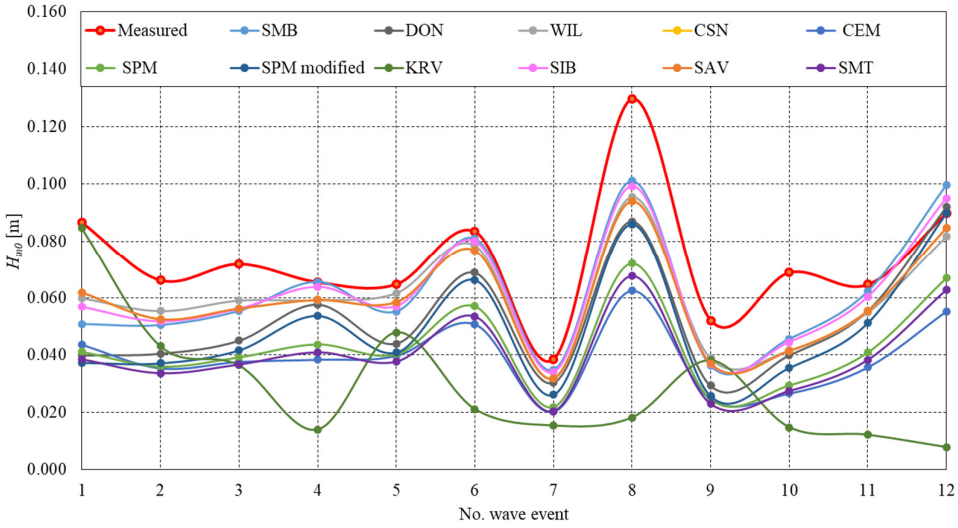



**Fig. 14.** Comparison of measured and calculated wave heights – detail (without JON, WIL revisited and CEM modified) (Table 6).

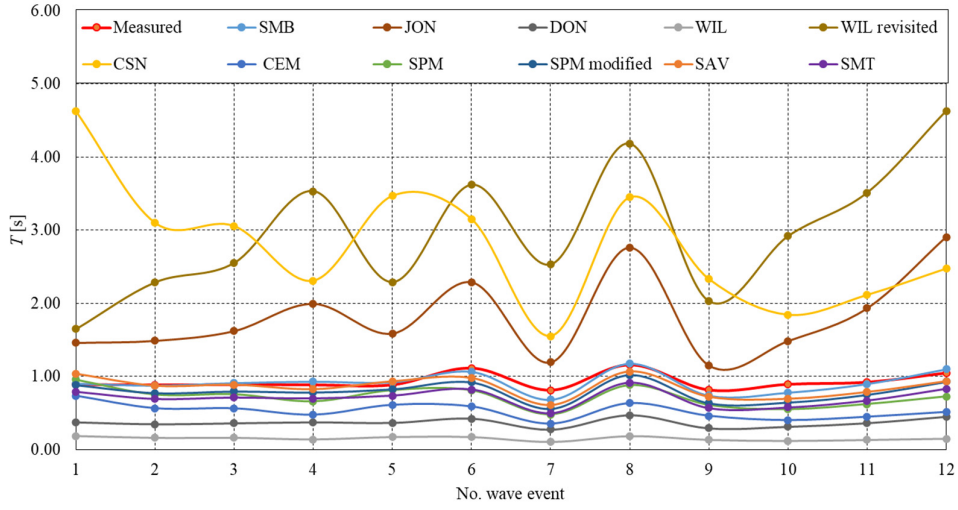



**Fig. 15.** Comparison of measured and calculated wave periods (Table 7).

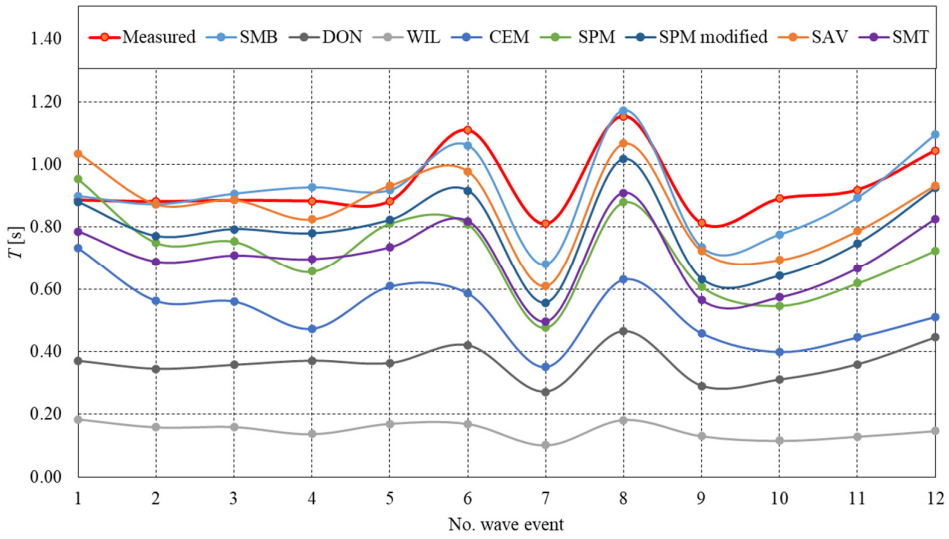



**Fig. 16.** Comparison of measured and calculated wave periods – detail (without CSN, JON, and WIL revisited) (Table 7).

underestimation or overestimation of measured values, sometimes by even more than 50 percent of wave height or wave period, affected empirical equations primarily in the case of small waves with a height of 15 cm and at wind speeds under10 m/s (Table 6 and 7).

Model efficiency was evaluated using the Nash-Sutcliffe efficiency coefficient (NSE), which determines the relative magnitude of the residual variance compared to the measured data variance. The NSE indicates how well the plot of observed versus simulated data fits the 1:1 line. *NSE* = 1 corresponds to a perfect match between the model and the observed data. *NSE* = 0 indicates that the model predictions are as accurate as the mean of the observed data. Inf < *NSE* < 0 indicates that the observed mean is a better predictor than the model. (Nash and Sutcliffe, 1970). Two coefficients related to the determination of the height and period of the wave were analysed:

$$N_H = 1 - \left[\frac{\sum_{i=1}^{12}(H_i - \overline{H_t})^2}{\sum_{i=1}^{12}(H_i - \widehat{H_t})^2}\right] \tag{50}$$

$$N_T = 1 - \left[\frac{\sum_{i=1}^{12}(T_{ci} - \overline{T_{ct}})^2}{\sum_{i=1}^{12}(T_{ci} - \widehat{T_{ct}})^2}\right] \tag{51}$$

where $H_i$ and $\overline{H_t}$ are the predicted and observed wave heights $H_{m0}$ [m], $\widehat{H_t}$ expresses the average of the observed wave heights $H_{m0}$ [m], $T_{ci}$ and $\overline{T_{ct}}$ are the predicted and observed wave periods [s], and Tc and $\widehat{T_{ct}}$ are the averages of wave periods [s] (Table 6). The results of the Nash-Sutcliffe model efficiency coefficient are listed in Table 8.

The calculated wave heights $H_{m0}$ [m/s] were verified based on the heights of the predicted and measured waves, where the minimum of the root-mean-square error (RMSE) was used as the criterion:

$$RMSE_{Hm0} = \sqrt{\sum_{i=1}^{n=12}\frac{(H_{m0i} - \overline{H_{m0i}})^2}{n}} = \min \tag{52}$$

where $H_{m0i}$ and $\overline{H_{m0i}}$ are the predicted and observed wave heights [m] (Table 6).

The calculated wave periods $T$ [s] were verified based on the periods of the predicted and measured waves, where the minimum of the root-mean-square error (RMSE) was used as the criterion:

$$RMSE_T = \sqrt{\sum_{i=1}^{n=12}\frac{(T_{ci} - \overline{T_{ci}})}{n}} = \min \tag{53}$$

where $T_{ci}$ and $\overline{T_{ci}}$ are the predicted and observed periods of waves [s] (Table 7).

The analysis of the predictive skills of the models was carried out using the Nash-Sutcliffe efficiency coefficient, ranging from 0.417 to –194.593 for predicting the height of waves, and from 0.66 to –426.429 for the prediction of wave period (Table 8). The Bretschneider (SMB) model or its modification (SIB) indicates good agreement between measured and calculated wave characteristics in the Hulín gravel pit with an average wind speed range of up to 8 m/s and wave heights of up to 15 cm. A significant proportion of the models underestimated wave height prediction and wave period prediction.

**Table 8.** The resulting Nash-Sutcliffe model efficiency coefficients (Equation 50 and Equation 51) and round mean square errors (Equation 52 and Equation 53).

| Parameter | SMB | WIL | WIL rev. | JON | DON | SPM | CSN | CEM | CEM mod. | SPM mod. | KRV | SIB | SAV | SMT |
|---|---|---|---|---|---|---|---|---|---|---|---|---|---|---|
| | | | | | | | ***NSE*** | | | | | | | |
| $N_{Hm0}$ | 0.350 | 0.398 | –194.593 | –89.59 | –0.358 | –3.916 | 0.366 | –1.81 | –65.66 | –0.64 | –5.06 | 0.417 | 0.366 | –1.642 |
| $N_T$ | 0.66 | –53.962 | –426.429 | –87.72 | –27.69 | –4.37 | –360.64 | –14.61 | – | –1.17 | – | – | –0.257 | –3.818 |
| | | | | | | | ***RMSE*** | | | | | | | |
| $RMSE_{Hm0}$ | 0.017 | 0.017 | 0.304 | 0.207 | 0.025 | 0.033 | 0.017 | 0.036 | 0.178 | 0.028 | 0.053 | 0.017 | 0.017 | 0.0354 |
| $RMSE_T$ | 0.062 | 0.787 | 2.196 | 1.000 | 0.569 | 0.246 | 2.020 | 0.419 | – | 0.157 | – | – | 0.119 | 0.233 |

## 4 CONCLUSION

The most suitable empirical spectrum for the Hulín small, closed reservoir and for other reservoirs with a similar shape corresponds to the Bretschneider spectrum with parameters set at $N$ = 3.8 [–] and $M$ = 9.0 [–]. However, the Bretschneider spectrum (and all of the other empirical spectra tested) does not provide the correct $S^{+}(\omega)$ energy values for low-frequency and low-altitude waves. From the results of this study it can be concluded that in the case of the Hulín gravel pit at the most stressed bank on a run-up fetch length of 450–1,400 m, there can be no balance between high-frequency waves and a fully developed Bretschneider spectrum.

A comparison of measured and predicted wave heights and periods calculated from Equations (24–44) is shown in Table 6. The best fit of $H_{m0}$ is provided by the SIB formula (27) with RMSE = 0.017, while the same order of magnitude is provided by the formula used by WIL, CSN, SAV, and SMB with a predictive RMSE of about 0.017. An analysis of the predictive skills of the models was then carried out using the Nash-Sutcliffe efficiency coefficient, which indicates that the best model for the prediction of wave height is the SIB model (Sibul, 1955), with $N_{Hm0}$ = 0.417. Other models mentioned above exhibited $N_{Hm0}$ = 0.398 – 0.350. Rather worse results (with RMSE 0.304) were provided by Equation (30) from Wilson (1965). A comparison of the results shows that the assessed empirical equations may underestimate or overestimate measured values, sometimes by even more than 5 times.

The comparison of obtained wave periods $T$ with predicted wave periods provides somewhat worse results (Table 7, Figure 15, and Figure 16). The best fit of $T$ provides the SMB formula Equation (24) with RMSE 0.064. It is the only model with predictive capabilities that is more accurate than the average of the observed data, with $N_T$ = 0.66. Rather worse results (with RMSE 2.196) were provided by Equation (31) from Wilson (1965). A comparison of the results shows that the assessed empirical equations may overestimate measured values, sometimes by even more than 4 times.

The best prediction of the wave height is provided using SIB, which is a modification of SMB, and the best prediction of the period is provided using SMB Equation (24) (Sverdrup and Munk, 1947; Bretschneider, 1959). The calculations show that the findings support the hypothesis that the Bretschneider spectrum existed on the Hulín lagoon (Table 3; Figure 7). It would be advisable to conduct further measurements on other water reservoirs where there is enough space for the high-frequency spectrum to emerge in order to guarantee the clarity of the data. It would be appropriate to perform more continuous measurements on other small closed reservoirs to verify the assumptions stated in the paper. To determine wave height in the shallow zone, new measurements (with depths of less than 2 m) must be taken, assessed, and compared with the available empirical equations. To adjust the accuracy of the empirical equations in the prediction of wave height and period, regression analysis should be performed in cases when there is enough measured data.

*Acknowledgements.* The paper is a part of the project FAST-S-22-8005 Spectral analysis of oscillating wind waves on water reservoirs as a part of adaptation to climate change and FAST-S-23-8233 Sensitivity analysis of selected input parameters of numerical models in hydraulic calculations.

## REFERENCES

Alves, J.H.G.M., Banner, M.L., Young, I.R., 2003. Revisiting the Pierson-Moskowitz Asymptotic Limits for Fully Developed Wind Waves. Journal of Physical Oceanography, 33, 7, 1301–1323.

Bretschneider, C.L., 1959. Wave variability and wave spectra for wind-generated gravity waves. Technical Memorandum No. 118. Beach Erosion Board, U.S. Army Corps of Engineers, 196 p.

Brodtkorb, P.A., Johannesson, P., Lindgren, G., Rychlik, I., Rydén, J., Sjo, E., 2000. WAFO – a Matlab toolbox for analysis of random waves and loads. Paper no. ISOPE 2000-GFC-02, 8 p.

BS-MS, 1993. British Standard, Maritime Structures (BS-MS). Part 1: Code of practice for general criteria. BS 6349-1:200.

Carter, D.J.T., 1982. Prediction of wave height and period for a constant wind velocity using the JONSWAP results. Ocean Engineering, 9, 1, 17–33.

CAS, 2022. Institute of Atmospheric Physics. Available: http://vitr.ufa.cas.cz/male-vte/ (accessed on 11 November 2022).

CSN 75 0255, 1988. Calculation of Wave Effects on Hydrotechnic Structures on Water Reservoirs. Czechoslovakia, 32 p. (In Czech). Available online: http://technicke-normy-csn.cz/750255-csn-75-0255_4_31249.html (accessed on 11 November 2022).

Donelan, M.A., 1980. Similarity theory applied to the forecasting if wave heights, periods and directions. In: Proceedings Canadian Coastal Conference. National Research Council, Canada.

Etemad-Shahidi, A., Kazeminezhad, M.H., Mousavi, S.J., 2009. On the prediction using simplified methods. Journal of Coastal Research, 1, Special Issue 56, 505–509.

Hanslian, D., Hošek, J., Chládová, Z., Pop, L., 2013. Wind conditions in the Czech Republic at a height of 10 m above the surface I. (In Czech.) Available: https://oze.tzb-info.cz/vetrna-energie/9770-vetrne-podminky-v-ceske-republice-ve-vysce-10-m-nad-povrchem- i (accessed on 11 November 2022).

Hasselmann, K., Barnett, T.P., Bouws, E., Carlson, H., Cartwright, D.E., Enke, K., Ewing, J.A., Gienapp, H., Hasselmann, D.E., Kruseman, P., Meerburg, A., Muller, P., Olbers, D.J., Richter, K., Sell, W., Walden, H., 1973. Measurements of Wind-Wave Growth and Swell Decay during the Joint North Sea Wave Project (JONSWAP). UDO 551.466.31. ANE German Bight, Deutsches Hydrographisches Institut, Hamburg, Germany, 94 p.

Choi, B.-Y., Jo, H.-J., Lee, K.-H., Byoun, D.-H., 2018. Development of Wind Induced Wave Predict Using Revisited Methods. Journal of Advanced Research in Ocean Engineering, 4, 3, 124–134.

Kazeminezhad, M.H., Etemad-Shahidi, A., Mousavi, S.J., 2005. Application of fuzzy inference system in the prediction of wave parameters. Ocean Engineering, 32, 14–15, 1709–1725.

Klaus, H., Olbers, D.J., 1973. Measurements of Wind-Wave Growth and Swell Decay During the Joint North Sea Wave Project (JONSWAP), pp. 2–95.

Kotaška, S., 2019. Measurement of wind oscillatory waves on reservoir. Master's Thesis. Brno University of Technology. Faculty of Civil Engineering. Department of Water Structures Brno, 101 p. (In Czech.) Available online: http://hdl.handle.net/11012/137529. (accessed on 11 November 2022).

Krylov, Y.M., Strekalov, S.S., Tsyplukhin, V.F., 1976. Wind Waves and Their Impact on Structures. Gidrometeoizdat, Leningrad, 255 p. (In Russian.)

Le Méhauté, B., 1976. An Introduction to Hydrodynamics and Water Waves. Springer-Verlag.

Mahmood, M.F, Henderson, D., Segur, H., 2010. Water Waves Theory and Experiment. In: Proceedings of the Conference. World Scientific Publishing Co., River Edge, NJ, USA, pp. 79–81.

Marinet, 2015. Best Practice Manual for Wave Simulation. WP2: Marine Energy System Testing – Standardisation and Best Practice. Version 3, 47 p.

MATLAB, 2022. Matlab version 9.12.0 (R2022a). The MathWorks Inc, Natick, Massachusetts.

McCormick, M.E., 1998. On the Use of Wind-Wave Spectral Formulas to Estimate Wave Energy Resources. Journal of Energy Resources Technology, 120, 314–317.

Michel, W.H., 1968. Sea Spectra Simplified. In: Proc. Meeting of the Gulf Section of the Society of Naval Architects and Marine Engineers.

Nash, J.E.; Sutcliffe, J.V., 1970. River flow forecasting through conceptual model. Part 1 – A discussion of principles. Journal of Hydrology, 10, 282–290.

NDBC, 2022. National Data Buoy Center. Available: https://www.ndbc.noaa.gov (accessed on 11 November 2022).

OCADIJ, 2002. Overseas Coastal Area Development Institute of Japan (OCADIJ). Technical Standards and Commentaries for Port and Harbor Facilities in Japan. Japan, 664 p.

Ochi, M.K., Hubble, E.N., 1976. Six-parameter wave spectra. In: Proc. Int. Conf. Coastal. Eng. 1, 15, pp. 301–328.

Owen, M.W., Steele, A.A.J., 1988. Wave prediction in reservoirs, comparison of available methods. Report EX 1809, HR Wallingford, 110 p. Available online: https://eprints.hrwallingford.com/179/ (accessed on 11 November 2022).

Ozeren, Y., Wren, D., 2009. Predicting wind-driven waves in small reservoirs. American Society of Agricultural and Biological Engineers (ASABE), 51, 5, 1599–1612.

Pelikán, P., Marková, J., 2013. Wind effect on water surface of water reservoirs. Acta Univ. Agric. Silvic. Mendel. Brun., 61, 6, 1823–1828.

Pelikán, P., Šlezingr, M., 2015. Parameters of wind-driven waves on Nove Mlyny water reservoir. In: Proc. Conf. Water Management and Hydraulic Engineering 2015. Institute of Water Structures, FCE, BUT, Brno, Czech Republic, pp. 55–64.

Pelikán, P., Koutný, L., 2016. Hindcast of wind driven wave heights in water reservoirs. Soil Water Res., 11, 3, 205–211.

Pelikán, P., Hubačíková, V., Kaletova, T., Fuska, J., 2020. Comparative assessment of different modelling schemes and their applicability to inland small reservoirs: A Central Europe case study. Sustainability, 12, 14 pp.

Pelikán, P., Špano, M., Čejda, M., 2020. Equipment for measuring and transmitting data of wind oscillating waves on water reservoirs (In Czech: Zařízení pro měření a přenos dat větrových oscilačních vln na vodních nádržích.). Utility model, Office industry property Czech Republic, 7 p. Available online: https://isdv.upv.cz/doc/FullFiles/UtilityModels/FullDocuments/FDUM0034/uv034513.pdf (accessed on 11 November 2022).

Phillips, O.M., 1958. The equilibrium range in the spectrum of wind-generated waves. J. Fluid Mech., 4, 426–434.

Říha, J., Špano, M., 2012. The influence of current on the height of wind wave run-up, a comparison of experimental results with the Czech National Standard. J. Hydrol. Hydromech., 60, 3, 174–184.

Saville, T., McClendon, E.W., Cochran, A.L., 1962. Freeboard allowances for waves in inland reservoirs. Journal of Waterways and Harbors Division, ASCE, 88, 2, 93–124.

Sibul, O., 1955. Laboratory Study of the Generation of Wind Waves in Shallow Water. Technical Memo No. 72. U.S. Army Corps of Engineers Beach Erosion Board, p. 35.

Smith, J.M., 1991. Wind-Wave Generation on Restricted Fetches. Miscellaneous Paper CERC-91-2. US Army Waterways Experiment Station, Vicksburg, MS.

SPM, 1977. United States Army Corps of Engineers and Coastal Engineering Research Center (U.S. Army, 1977). Shore Protection Manual (SPM). Department of the Army, Waterways Experiment Station, Corps of Engineers, Coastal Engineering Research Center.

SPM, 1984. United States Army Corps of Engineers and Coastal Engineering Research Center (U.S. Army, 1984). Shore Protection Manual, Department of the Army, Waterways Experiment Station, Corps of Engineers, Coastal Engineering Research Center, 652 p.

Stoica, P., Moses, R., 2005.Spectral analysis of signals. Prentice Hall, Upper Saddle River, New Jersey 07458, USA, 447 p. ISBN 0-13-113956-8.

Sverdrup, H.V., Munk, W.H., 1947. Wind, sea, and swell: Theory of relations for forecasting. Hydrographic Office Pub. 60, US Navy.

Špano, M., 2019. Protection of embankments and banks against action caused by oscillatory wind waves. In: Proceedings of the ICOLD 2019 Symposium 9.-14.6.2019 Ottawa, Canada. Sustainable and Safe Dams Around the World. ICOLD/CIGB. Paris, France, pp. 3095–3102.

Špano, M., Duchan, D., Kotaška, S., Skřečková, K., Prokopová, E., Pelikán, P., Hrůza, O., Seidl, R., Dvořáková, S., Švancara, J., Čejda, M., 2020. Protection of water structures and natural banks against the effects of oscillating wind waves. (In Czech: Ochrana konstrukcí vodních staveb a přirozených břehů před účinky oscilačních větrových vln.) Partial report of TH03030182: Protection of hydraulic structures against action caused by oscilatory wind waves. Brno: BUT, TAČR No. I/2020, 56 p.

Špano, M., Duchan, D., 2021. Threat to embankments and natural banks posed by oscillatory wind waves. Gospodarka wodna, 873, 9, 10–16.

Špano, M., Bornschein, A., Pohl, R., Říha, J., Schuttrumpf, H., 2022. Wave run-ups and overtopping affected by oblique wave approaches and currents. Slovak Journal of Civil Engineering, 30, 2, 12–21.

Torsethaugen, K., 1993. Two peak wave spectrum model. In: Proceedings of the International Conference on Offshore Mechanics and Arctic Engineering – OMAE, (2), pp. 2–10.

Vincent, C.L., Demirbilek Z., Weggel, J.R., 2002. Coastal Engineering Manual: Part II. Coastal Hydrodynamics. Engineer Manual 1110-2-1100. U.S. Army Corps of Engineers, Washington, D.C., 623 p.

WAFO GROUP, 2017. A Matlab Toolbox for Analysis of Random Waves and Loads. Tutorial for WAFO version 2017. Lund University, Faculty of Engineering, Centre for Mathematical sciences, Mathematical statistics, 195 p.

Wilson, B.W., 1955. Graphical approach to the forecasting of waves in moving fetches. U.S. Army. Tech. Mem., No. 73. Beach Erosion Board, Corps of Engrs., 31 p.

Wilson, B.W., 1965. Numerical prediction of ocean waves in the North Atlantic for December, 1959. Deutsche Hydrographische Z., 18, 3, 114–130.

Yarde, A.J., Banyard, L.S., Allsop, N.W.H., 1996. Reservoir dams: wave conditions, wave overtopping and slab protection. HR Wallingford, no. CAS 0021, 62 p.

Received 16 January 2023
Accepted 8 August 2023